ARTICLE

Medioapical contractile pulses coordinated between cells regulate *Drosophila* eye morphogenesis

Christian Rosa-Birriel[1] , Jacob Malin[1] , and Victor Hatini[1]

Lattice cells (LCs) in the developing *Drosophila* retina change shape before attaining final form. Previously, we showed that repeated contraction and expansion of apical cell contacts affect these dynamics. Here, we describe another factor, the assembly of a Rho1-dependent medioapical actomyosin ring formed by nodes linked by filaments that contract the apical cell area. Cell area contraction alternates with relaxation, generating pulsatile changes in cell area that exert force on neighboring LCs. Moreover, Rho1 signaling is sensitive to mechanical changes, becoming active when tension decreases and cells expand, while the negative regulator RhoGAP71E accumulates when tension increases and cells contract. This results in cycles of cell area contraction and relaxation that are reciprocally synchronized between adjacent LCs. Thus, mechanically sensitive Rho1 signaling controls pulsatile medioapical actomyosin contraction and coordinates cell behavior across the epithelium. Disrupting the kinetics of pulsing can lead to developmental errors, suggesting this process controls cell shape and tissue integrity during epithelial morphogenesis of the retina.

Introduction

Morphogenesis of the *Drosophila* retina involves changes in cell shape, size, and junction length that seem largely transient. Through this process, which unfolds over tens of hours, epithelial cells achieve their precise number, shape, and arrangement. The result is a tessellated structure composed of ~800 nearly identical ommatidia (Cagan and Ready, 1989). This process is a model for understanding morphogenesis of differentiated cells forming a mature organ. Each ommatidium consists of four central cone cells, surrounded by two large semicircular primary (1°) cells. These are surrounded by lattice cells (LCs) and mechanosensory bristles (Fig. 1 A). Of these, the LCs exhibit a particularly intricate developmental sequence in which they intercalate to arrange in a single file between ommatidia, extra LCs are pruned, and remaining cells undergo dramatic shape changes according to their location (Cagan, 2009; Carthew, 2007; Johnson, 2021).

The initial arrangement of cells in ommatidia is controlled by differential adhesion (Bao and Cagan, 2005; Bao et al., 2010; Hayashi and Carthew, 2004). After the intercalation of LCs, certain cytoskeletal networks are preferentially associated with a subset of LCs' contacts. Specifically, we showed that contractile junctional actomyosin networks assemble at and contract the LC–LC contacts. These contractile networks are counterbalanced by protrusive branched actin networks that assemble along the same contacts with reciprocal dynamics (Del Signore et al., 2018; Malin et al., 2022). This interplay of contractile and protrusive forces along cell contacts guides, at least in part, their movements and prevents errors in cell shaping and arrangement.

Medioapical actomyosin networks have been observed during epithelial remodeling in several processes in *Drosophila*, including gastrulation, germband extension, and dorsal closure (Azevedo et al., 2011; Blanchard et al., 2010; Fernandez-Gonzalez and Zallen, 2011; Martin et al., 2009; Rauzi et al., 2010; Solon et al., 2009). In those processes, medioapical actomyosin networks pulse—that is, they repeatedly assemble and disassemble. Disrupting pulsing affects cell behavior and epithelial organization. However, these early developmental processes fundamentally differ from the remodeling of the retina. They entail massive reorganization of cells that takes place over the time course of tens of minutes compared with the precise refinement of the retina, which takes tens of hours. Furthermore, the pulsation typically displays a ratcheting characteristic, in which relaxation after constriction is only partial and the cells never revert to their original shape. In contrast, in the retina, there is no obvious ratcheting characteristic to cell-shape changes.

Cell movement and shape changes, however, are clearly critical for generating the very precise organization of the retina because errors occur when they are perturbed (Blackie et al.,

[1]Department of Developmental, Molecular and Chemical Biology, Program in Cell, Molecular and Developmental Biology, Program in Genetics, and Program in Pharmacology and Experimental Therapeutics, Tufts University School of Medicine, Boston, MA, USA.

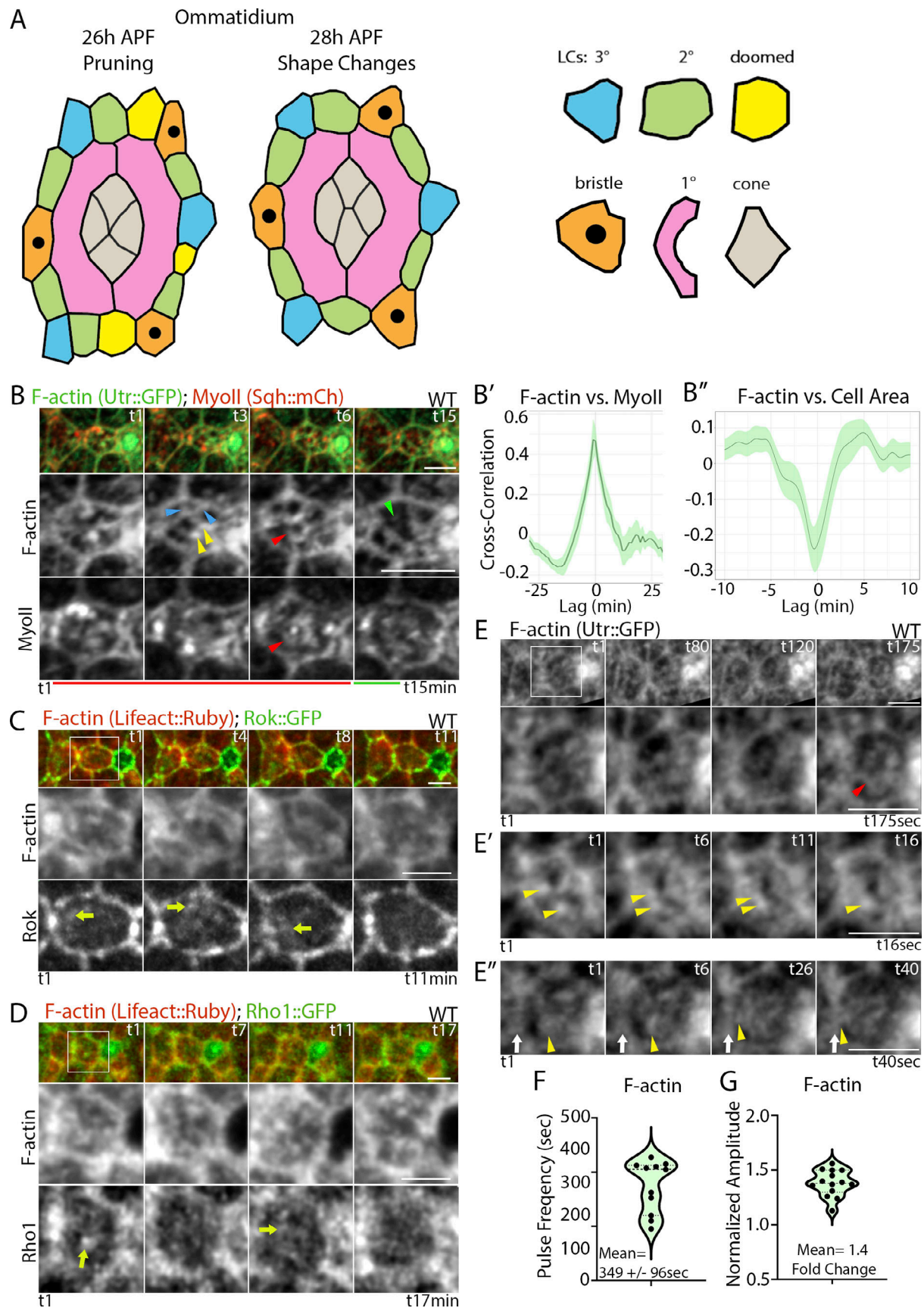Correspondence to Victor Hatini: victor.hatini@tufts.edu.

Figure 1. **Pulsatile medioapical actomyosin dynamics correlate with cell area changes during epithelial remodeling. (A)** Left: During remodeling of ommatidia, the 2° LCs narrow and elongate with 3° LCs compact to form alternating corners. Right: Key for cell types. **(B)** Medioapical actomyosin dynamics in

LCs during cell shape changes. Top: Snapshots of a lattice edge. Bottom: Zoomed-in images of F-actin and MyoII. In the first three time points, the cell is contracting (red bar below), and in the last, it is expanding (green bar). F-actin is present in nodes (yellow arrowheads) that are moving and appear to increase during contraction. The nodes form a ring-like structure (red arrowhead) connecting to the cell surface (blue arrowheads). The ring disassembles and remodels during expansion (green arrowhead points to a gap forming in the ring at t15). **(B′ and B″)** Time-shifted Pearson's correlation charts (N = 11 cells from three eyes). Solid line, mean R-value at each time shift; Green band, standard error of the mean, here and in subsequent figures. **(B′)** Medioapical F-actin and MyoII accumulate in synchrony, positively correlating with 0 time lag. **(B″)** F-actin and cell area negatively correlate, with peak F-actin occurring 15 s before peak contraction. **(C)** Rok is present and moving in LCs. Top: Snapshots of a lattice edge. Bottom: Zoomed-in views of boxed area. Yellow arrows: Medioapical foci of Rok accumulation. **(D)** Rho1 is present and moving. Top: Snapshots of a lattice edge. Bottom: Zoomed-in views of F-actin and Rho1 in an LC. Yellow arrows: Foci of Rho1 accumulation. **(E–E″)** At higher temporal resolution, three behaviors of the medioapical actomyosin network in LCs are discernable (Video 1). **(E)** Enrichment of medioapical F-actin precedes the assembly of a medioapical ring (red arrowhead). **(E′)** Movement and fusion of F-actin nodes (yellow arrowheads). **(E″)** Movement of nodes (yellow arrowheads) and fusion with the junctional actomyosin network (white arrow). **(F)** Medioapical F-actin pulse frequency in WT 2° LCs is ∼6 min (349 ± 96 s, N = 11 cells from three eyes). **(G)** On average, medioapical F-actin levels are 1.4-fold higher at their peak than at their trough levels (N = 14 cells from three eyes). Scale bar = 3 μm.

2020, 2021; Del Signore et al., 2018; Johnson et al., 2008; Larson et al., 2008; Letizia et al., 2019; Malin et al., 2022; Seppa et al., 2008). Thus, a major challenge is identifying mechanisms that regulate cell dynamics and understanding their impact on force generation, force transmission, and the eventual attainment of specific cell shapes. Likewise, little is known about if and how neighboring cells affect each other in this process. A medioapical actomyosin network is known to be present in the developing fly retina, but its regulation and role in coordinating cell shape changes across an epithelium remain unexplored (Blackie et al., 2020).

Here, we used *Drosophila* LCs to investigate the organization, dynamic properties, roles, and regulation of the medioapical actomyosin network in LC remodeling using high-resolution live imaging and laser ablation combined with genetic tests of gene function. We found a pulsatile medioapical actomyosin network, whose assembly in a ring-like structure promotes the transient, anisotropic contraction of LCs. In addition to identifying regulators of this network, our experiments surprisingly revealed the role of medioapical actomyosin networks in creating and responding to mechanical interactions between neighboring cells. Our work illuminates the operation and regulation of medioapical actomyosin networks through cells' mechanical state and interaction between neighboring cells. Overall, our data provide evidence that biochemical and mechanical signals regulate Rho1 function to rebalance forces in the epithelium, control cell shape and cell rearrangements, and maintain tissue integrity.

Results

A dynamic medioapical actomyosin network assembles during LC remodeling

The developing fly retina is a model for understanding how force-generating cytoskeletal networks control cell shape, cell-to-cell interactions, and tissue patterns. To examine the medioapical actomyosin network during lattice remodeling, we live-imaged F-actin using the actin-binding domain of Utrophin tagged with GFP (Utr::GFP), together with Spaghetti Squash (Sqh), the regulatory light chain of non-muscle Myosin II (MyoII), tagged with mCherry (MyoII::mCh). In time-lapse movies, imaging a Z-stack every 60 s, we found that F-actin and MyoII accumulated in particles that flowed from the cell surface toward the cell's medioapical region as the apical area exhibited

pulsing shape changes (Fig. 1 B). Hinted at in low-resolution imaging (Fig. 1 B) and more clearly visible at higher temporal or spatial resolution (Fig. 2 A), an actomyosin ring structure was transiently present (red arrowheads). To study how medioapical actomyosin accumulation and cell area changes relate over time, we used time-resolved Pearson's correlation analysis. This method calculates a correlation coefficient for data pairs from two-time series, varying the time delay between them. The resulting coefficients are plotted against the time lag on a graph, showing the strength and direction of their relationship. This analysis not only detects correlations between synchronous endpoints but also between endpoints that precede or follow each other in time, revealing the temporal lag between them. Time correlation analysis confirmed that medioapical F-actin and MyoII intensity increased synchronously, with no lag, suggesting they coassemble to form a contractile actomyosin network (Fig. 1 B′ and Fig. S1, A–B′, R = 0.4400). We also observed fluctuations in the LCs' apical area (Fig. 1 B) and asked if they correlated with fluctuations in actomyosin levels. We found a significant negative correlation between medioapical F-actin and LCs' apical area (Fig. 1 B″ and Fig. S1 B″, R = −0.2706 at −15 s). F-actin peaked 15 s before peak apical constriction, consistent with the idea that an increase in medioapical actomyosin levels exerts tension on the apical cell perimeter leading to a reduction in the apical cell area.

The Rho1 Rho GTPase and Rho-kinase (Rok) control actomyosin network assembly and contraction (Dawes-Hoang et al., 2005; Magie et al., 1999; Mizuno et al., 1999; Mulinari et al., 2008; Warner and Longmore, 2009a, 2009b). Therefore, we examined the accumulation of GFP-tagged Rho1 and Rok reporters relative to F-actin marked with the F-actin–binding peptide Lifeact tagged with Ruby fluorescent protein (Lifeact:: Ruby). We found that both Rho1 and Rok are moving and accumulating medioapically (Fig. 1, C and D, yellow arrows), suggesting that the two proteins are positioned to control medioapical actomyosin dynamics.

To better understand the dynamic properties of the medioapical actomyosin and its structure, we imaged the network at a higher temporal resolution, obtaining an image stack every 5 s (Video 1). The medioapical actomyosin peaked in intensity approximately every 6 min (Fig. 1 F; 349 ± 96 s), with a 1.4-fold increase in F-actin levels from trough to peak in each cycle (Fig. 1 G). We found that during epochs of cell contraction, F-actin particles moved toward one another and merged to form
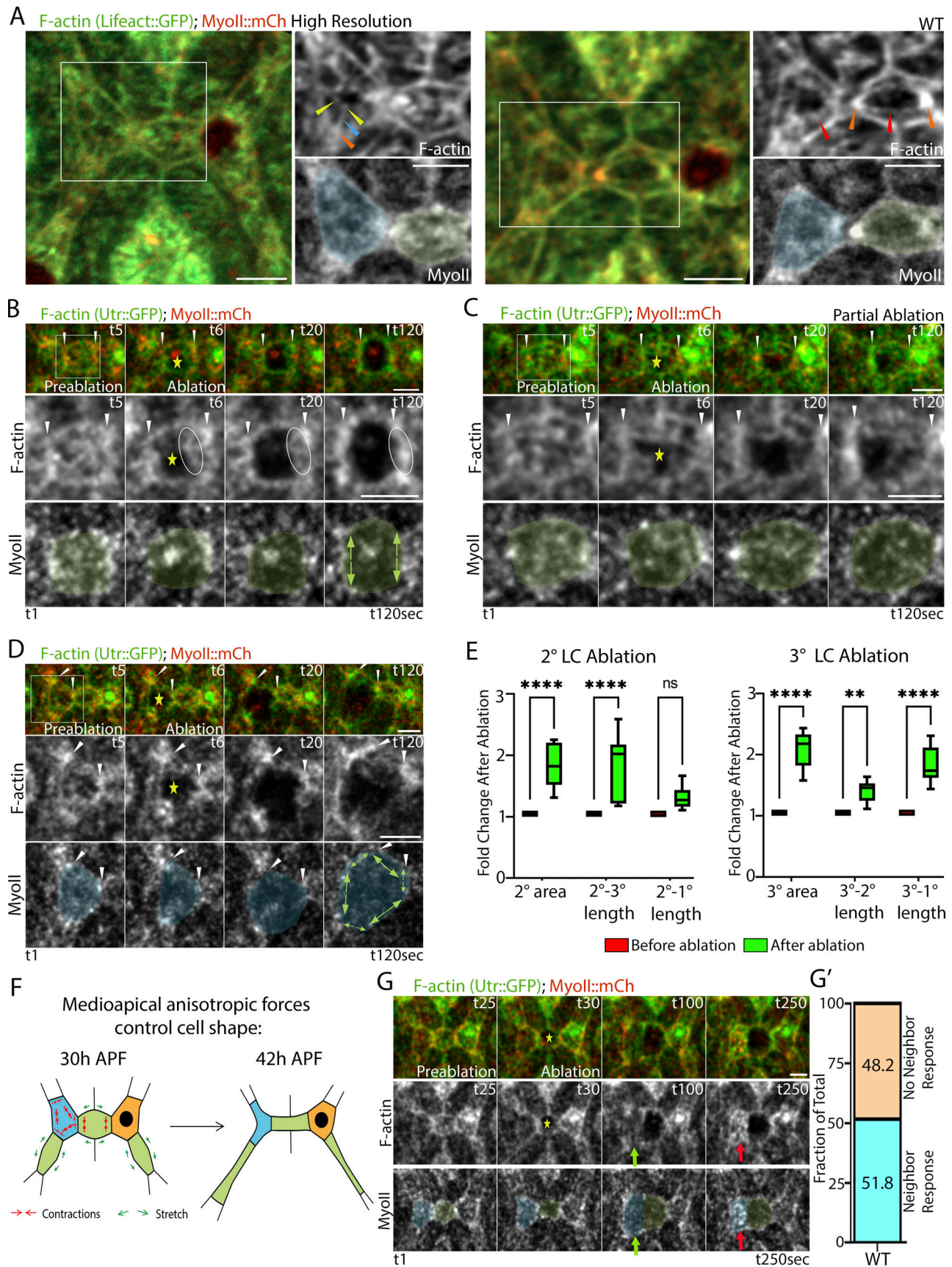
Figure 2. **The medioapical actomyosin network holds tension and mechanically links neighboring LCs. (A)** High-resolution Airyscan images of F-actin and MyoII from a time-lapse movie (representative ommatidia from six Airyscan movies). The 2° and 3° LCs are highlighted by the green and blue overlays,

Rosa-Birriel et al.
Biomechanical cell coordination in morphogenesis

Journal of Cell Biology
https://doi.org/10.1083/jcb.202304041

4 of 19

respectively. Left: Medioapical actomyosin nodes (yellow arrowheads) that form a ring structure are connected to nodes at the cell surface (orange arrowheads) via filamentous structures (blue arrowhead). Right: Medioapical actomyosin nodes form a ring structure (red arrowheads) that links to nodes at the cell surface (orange arrowheads). **(B–E)** Targeted ablations (Video 2) of medioapical actomyosin in LCs (marked with a yellow star) induce a rapid recoil of medioapical actomyosin and lead to apical cell area expansion. **(B)** Medioapical actomyosin ablation in 2° LCs induces preferential expansion of the LC–LC contact and actomyosin flow (tracked by the ellipse) toward LC–LC contacts (white arrows) concomitant with apical area relaxation (green overlay highlights the 2° LCs, green double arrows point to the direction of cell expansion). Top: Snapshots of a lattice edge from a time-lapse movie; Bottom: Zoomed-in views of F-actin and MyoII (N = 10 cells from three eyes). **(C)** Ablations in which only some medioapical actomyosin recoiled exhibit weaker apical area expansion (green overlay highlights the 2° LCs) (N = 3 partial ablations of 27 ablations). White arrowheads mark contacts with neighboring cells in the lattice. **(D)** Ablation of the medioapical actomyosin network in 3° LCs (highlighted by a blue overlay) induces a strong relaxation of the apical cell area and a preferential expansion of 3°-1° contacts compared with LC–LC (3°-2°) contacts (N = 10 cells from four eyes). White arrowheads point to LC–LC contacts. Green double arrows point to the direction of cell expansion. **(E)** Left panel: Fold change of the 2° LC area and cell–cell contacts after ablation. Two-way ANOVA was performed with Sídák's multicomparison to compare each data set before to after ablation. 2° LCs area after ablation versus before ablation, P < 0.0001, N = 10. 2°-3° contact length after ablation versus before ablation, P < 0.0001, N = 10. 2°-1° contact length after ablation versus before ablation, P = 0.1569, N = 10 from four eyes. Right panel: Fold change of the 3° cell area and cell–cell contact before and after ablation. 3° LCs area after ablation versus before ablation, P < 0.0001, N = 8 from four eyes. 3°-2° contact length after ablation versus before ablation, P = 0.0015, N = 8 from four eyes. 3°-1° contact length after ablation versus before ablation, P < 0.0001, N = 8 from four eyes. **(F)** A cartoon depicting the forces affecting cell shape inferred from the pattern of recoil of 2° and 3° LCs after ablation. Red arrows depict contractile forces, and their thickness represents their magnitude. Green arrows depict the passive stretching of the 2°-1° cell contacts in response to the contraction of the 3° LCs. **(G)** Left: Snapshots from a time-lapse movie of a lattice edge before and after 2° LC ablation. In the MyoII channel, the ablated 2° cell is highlighted in green and the adjacent non-ablated 3° LC in blue. After ablation (marked with a yellow star), the apical area of the neighboring 3° LC initially expands (green arrow). This is followed by an increase in medioapical actomyosin (red arrow) and cell area contraction. **(G')** Approximately half of the non-ablated neighboring LCs (14 cells out of 27 cells in nine eyes) assembled a robust medioapical actomyosin network and contracted after ablation of their neighboring cell. Scale bar = 3 μm.

larger particles organized into a ring-like structure, corresponding to peak intensity (Fig. 1, E and E'; and Video 1). As the ring disassembled, some particles disappeared while others flowed toward cell edges and merged with the junctional network (Fig. 1 E'', yellow arrowhead; Video 1). Taken together, these observations imply that medioapical actomyosin forms a contractile network composed of interconnected nodes that pull on one another and the cell surface in a process controlled by Rho1 and Rok.

Medioapical actomyosin exerts tension on the apical cell surface and is mechanically adaptive

Using high-resolution Airyscan confocal imaging, we examined the structure of the medioapical actomyosin network at higher spatial resolution in time-lapse movies (Fig. 2 A). This provided increased clarity to the presence of nodes (yellow arrowheads) that form the medioapical ring-like structure (red arrowheads) and filamentous structures (blue arrowhead) that linked nodes to other nodes and the cell surface or to LC–LC contacts (orange arrowheads). This architecture suggested that the network exerts tension on the cell surface and that LCs are mechanically linked through a dynamic supracellular medioapical actomyosin network anchored, in part, at LC–LC contacts.

To test the mechanical role of the medioapical actomyosin network, we ablated the network either partially or entirely and investigated the effects. First, we asked if ablated cells remained viable and mechanically active. We found that after ablation, the network quickly recoiled toward the cell surface and then reassembled within 8 min (Fig. S2, A and A'). In contrast to apical membrane wounds, which induce purse string formation and closure (Abreu-Blanco et al., 2012; Martin and Lewis, 1992; Wood et al., 2002), our ablations did not, indicating that ablated cells remained viable and mechanically active. After ablation of 2° LCs, we found that F-actin structures recoiled toward the cell periphery (Fig. 2 B). Concomitantly, we observed a rapid anisometric relaxation of the apical cell area preferentially parallel to LC–LC contacts (Fig. 2, B and C; and Video 2). The severing and recoil of the medioapical actomyosin network increased the 2° LCs' total area by approximately twofold, resulting from cell area expansion along the shorter axis, while the longer axis was not significantly affected (Fig. 2, B, C, and E, green double arrows). We next ablated the 3° LCs and observed a similar twofold increase in the apical cell area (Fig. 2, D and E; and Video 2). Additionally, we found that both the LC–LC (3°-2°) and 3°-1° contacts expanded, although 3°-1° contacts expanded more (Fig. 2 E, thin and thick green double arrows, respectively). Additionally, we compared the impact of ablating the medioapical actomyosin network in 2° LCs versus 3° LCs on cell contact expansion. Ablating the network in 2° LCs had a greater impact on 2°-3° contact expansion compared with the impact of ablating the network in 3° LCs. Conversely, ablating the network in 3° LCs had a greater impact on 1°-3° contact expansion compared with the impact of ablating the 2° LCs (Fig. S6). These mechanical responses imply that the medioapical actomyosin network contracts asymmetrically to preferentially shrink the LC-LC and 3°-1° contacts and guide the shape changes of the LCs. Overall, these recoil patterns indicate that in 2° LCs, the medioapical actomyosin network promotes the shortening of LC–LC contacts, while in 3° LCs, it preferentially shortens the 3°-1° contact and contributes to the shortening of LC–LC contacts (see model in Fig. 2 F).

We note a surprising non-autonomous effect of ablating the medioapical network in LCs. To study the effect on adjacent non-ablated cells, we imaged the process for several minutes after ablation. The ablation of an individual 2° LC initially resulted in the expansion of the adjacent LC (Fig. 2 G, green arrow). After this initial expansion, approximately half of the neighboring non-ablated LCs assembled a robust medioapical actomyosin network that contracted their apical cell area (red arrow; Fig. 2, G and G', ~52% response of N = 27). While the pulse duration in WT is ~6 min, maximal contraction occurred 98 ± 8 s after ablating the neighboring LC, indicating that the ablation

accelerated the pulse cycle. The response implies that LCs respond to the loss of tension from the adjacent cell by assembling medioapical actomyosin to restore tension.

Rho1 regulates the frequency and amplitude of medioapical actomyosin network assembly

We next investigated the effect of perturbing assembly of the medioapical actomyosin network during LC remodeling by manipulating Rho1. Expressing a dominant-negative Rho1 (Rho1[DN]) caused a general increase in apical cell areas and large fluctuations in cell area over time (Fig. 3 A). In these cells, junctional and medioapical F-actin were sparse and adherens junctions (AJs) were at least partially compromised (white arrow). Nevertheless, cell area contractions were observed and they were accompanied by increases in F-actin (red brackets). This manifested as a stronger correlation between medioapical F-actin accumulation and contraction of cell area compared with wild type (WT; Fig. 3 A′). These observations provide another line of evidence for the role and importance of medioapical actomyosin networks in controlling changes in apical cell area and accumulating in response to low tension.

To test whether Rho1 was sufficient to affect medioapical actomyosin dynamics, we transiently overexpressed WT Rho1 using the GAL4/GAL80[ts] system, successfully maintaining cell connectivity and tissue integrity. Rho1 overexpression altered the kinetics of medioapical actomyosin pulsing (Fig. 3, B and C; and Video 3). Rho1 overexpression also promoted the fusion and enlargement of medioapical F-actin nodes' by approximately threefold compared with WT cells (Fig. 3, B and B′; and Video 3). There was an increased F-actin pulse frequency (245 ± 50 s in Fig. 3, C and C′, compared with 349 ± 96 s in WT in Fig. 1 F) and amplitude (4.5-fold change, Fig. 3 C″, compared with 1.4-fold change in WT in Fig. 1 G). With Rho1 overexpression, there was a robust (Fig. 3 C‴ and Video 3) correlation between F-actin and cell area (R = −0.6508 at −15 s, compared to WT shown in Fig. 1 B″, R = −0.2706 at −15 s). These results imply that Rho1 activity is tightly regulated to control the frequency and amplitude of medioapical actomyosin assembly and contractility. Furthermore, cell recoil velocities in Rho1-expressing cells increased after ablating the medioapical actomyosin network, supporting this conclusion (Fig. S5, D and E).

Rho1 overexpression reveals cell-to-cell mechanical interactions

Following up on our observation that the medioapical actomyosin network appeared to be triggered to assemble by the loss of tension (Fig. 2 G and Fig. 3 A), we studied the behavior of neighboring cells with Rho1 overexpression, where there are strong changes in the apical cell area. We focused on the behavior of adjacent 2° LCs prior to completion of cell pruning. In this cell configuration, one LC shares only one contact with the neighboring LC and a second with a mechanosensory bristle, while the second LC shares a second contact with a flanking 3° cell. Thus, adjacent LCs are exposed to the minimum of possible mechanical inputs from neighboring LCs, allowing us to isolate the mechanical interactions between these cells while minimizing the relevance of other neighboring cells. Time-lapse

movies showed that a 2° LC contraction coincided with a two-step response in a neighboring 2° cell (Video 4). First, the second 2° LC disassembled its actomyosin network and expanded its apical area (Fig. 3 E at 210 s). Then, it reassembled the network and contracted its apical area (Fig. 3 E at 595 s). This, in turn, coincided with the same two-step response in the first 2° LC, resulting in alternating cycles of expansion and contraction in neighboring LCs. The peak expansion of a LC occurred 15 s after the maximal contraction of the adjacent LC (Fig. 3 E′, R = −0.2020). Thus, as one cell contracted, the other expanded, and vice versa (Fig. 3, E′ and F; and Video 4). We also observed inversely coordinated cycles of expansion and contraction between adjacent anterior and posterior cone cells and 1° cells (Fig. S3, A–D, respectively). Thus, the medioapical actomyosin network not only contributes to cell-autonomous contractions but also exerts a force on adjacent LCs that sets up anticorrelated cycles of contraction and expansion in adjacent cells.

Dynamic activation of MyoII and F-actin is required for tissue integrity and remodeling

A salient characteristic of apical cell-area contraction produced by the Rho1-dependent medioapical network is that it is pulsatile. These pulsing shape changes are not ratcheting, and they oscillate for hours. To investigate the importance of the pulsatile nature of this process, we expressed a constitutively active myosin light chain kinase (MLCK[CA], Fig. 4 and Video 5), which constitutively activates MyoII using the GAL4/GAL80[ts] system. We examined the AJs, sites of force transmission, in eyes that expressed MLCK[CA]. We live-imaged α-Catenin tagged with GFP (α-Cat::GFP) to highlight the AJs and found that they were fragmented compared with WT (Fig. 4, B and C). A subset of the LCs failed to intercalate and clustered around mechanosensory bristles (Fig. 4 C, arrows). We also observed cells that dramatically expanded their apical area, suggesting that they failed to hold tension exerted by the medioapical actomyosin network and were pulled by their neighbors, thus compromising tissue integrity (Fig. 4 C, asterisks). Examination of these ruptures revealed filamentous actin structures linking MyoII foci across the rupture (Fig. 4 F). Furthermore, we also observed that MLCK[CA] expression decreased cells' average apical area (Fig. 4 E). Live imaging with MyoII::mCh showed a high level of MyoII along the entire cell perimeter. Additionally, MyoII was seen enriched in a continuous medioapical ring, differing from the assembly of nodes in a ring seen in WT. This ring transiently formed and disappeared (Fig. 4 F′ and Video 5) on average every 10 min (Fig. 4 F″), and its assembly correlated with cell area contraction (Fig. 4 F‴, R = −0.2126). Thus, MLCK[CA] expression alters the organization and kinetics of the medioapical actomyosin network. This changes cell size, causes some cells to rupture, and results in disorganized epithelium.

Taking a complementary approach to perturbing pulsed medioapical actomyosin-dependent cell contraction, we expressed a constitutively active form of Dia (Dia[CA]), which assembles linear actin filaments downstream of Rho1. We expressed Dia[CA] transiently using the GAL4/GAL80[ts] system. First, we fixed Dia[CA]-expressing eyes and stained them for E-cad to examine the integrity of the AJs and epithelial organization.
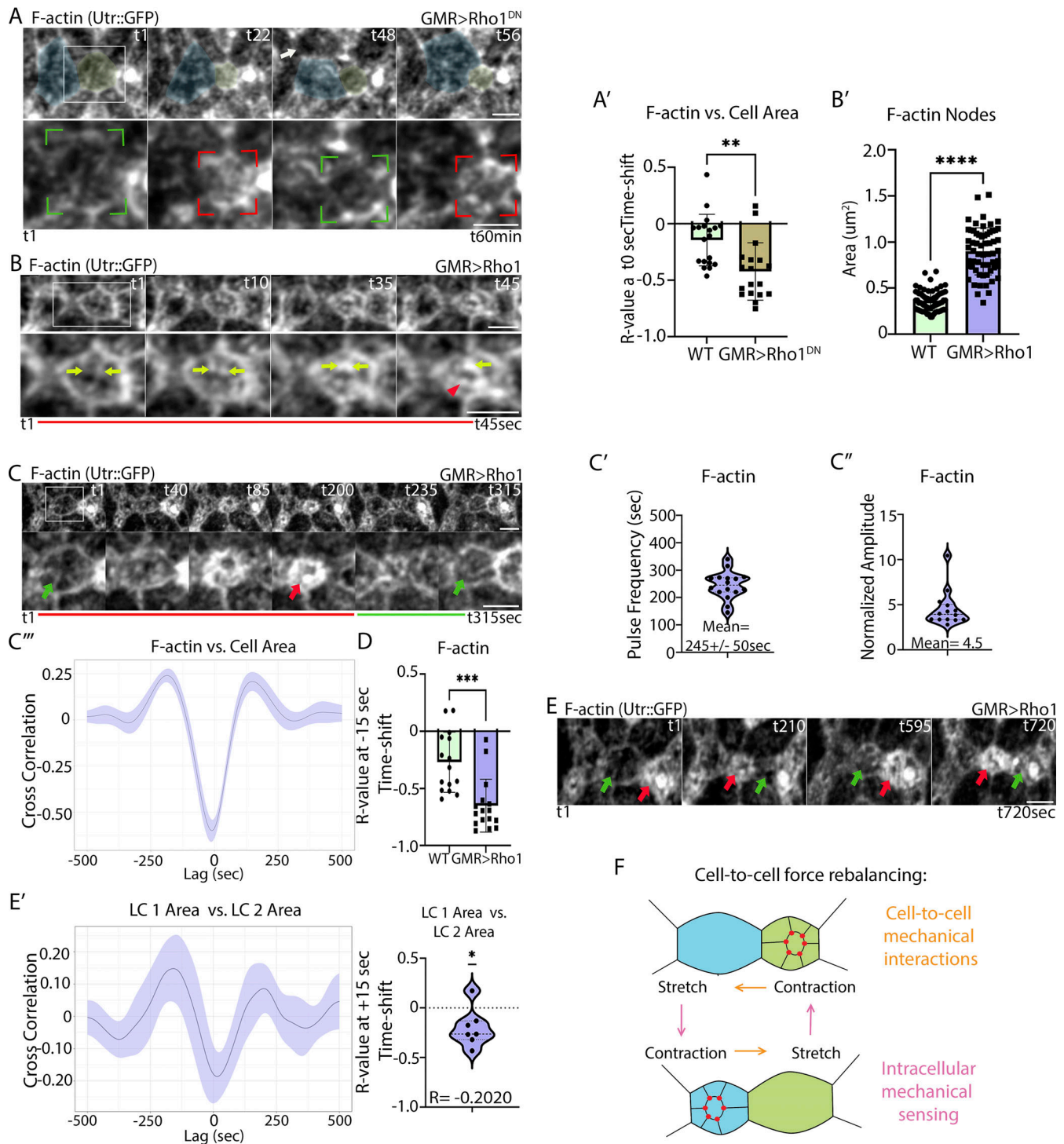
Figure 3. **Rho1 regulates actomyosin and cell area changes and reciprocal cytoskeletal and cell area changes in adjacent LCs. (A)** F-actin organization and dynamics in Rho1DN-expressing eyes. RhoDN expression disrupts actin organization, pulsatile actomyosin dynamics, and cell shape changes (see text for details). Top: Snapshots of a lattice edge. Blue and green overlays highlight adjacent 3° and 2° LCs, respectively. Bottom: Zoomed-in images of the 2° LC (boxed area). The bracketed green zones show low medioapical F-actin during cell area expansion, while bracketed red zones show increased F-actin during cell area contraction. Note an interruption of junctional actomyosin (white arrow). **(A′)** The negative correlation between medioapical F-actin levels and cell area contraction is stronger in GMR > Rho1DN compared with WT (N = 18 in WT, N = 19 in GMR > Rho1DN from three eyes each, t test, P = 0.0013). **(B and C)** Rho1 overexpression has a dramatic effect on pulsatile medioapical F-actin dynamics and cell area fluctuations (Video 3). **(B)** Time series montage shows F-actin node fusion (tracked by the yellow arrows) during medioapical F-actin ring formation (red arrowhead). **(B′)** F-actin nodes are on average 40% larger in GMR > Rho1 compared with WT (N = 70 nodes in WT, N = 60 in GMR > Rho1 from three eyes each, t test P < 0.0001). **(C)** A time series montage of a cell overexpressing Rho1 through a cycle of cell expansion (red bar) and contraction (green bar). Low F-actin intensity within expanded cells (green arrows), high F-actin intensity within contracted cells (red arrow). **(C′)** Medioapical F-actin pulse frequency in 2° LCs is accelerated (245 ± 50 s, N = 16). **(C″)** F-actin levels increase on average 4.5-fold in 2° LCs (N = 14) during contraction compared with 1.4-fold in WT (Fig. 1 G). **(C‴)** Time-shifted correlation shows that medioapical F-actin levels

correlate strongly with apical area contraction of 2° LCs. **(D)** The peak negative correlation between F-actin and cell area in Rho1-expressing eyes is significantly stronger than in WT (R = −0.6508 at peak correlation of −15 s, N = 15 from three eyes, t test P = 0.0002). **(E)** Contractile medioapical actomyosin dynamics and cell area fluctuations inversely coordinate between neighboring 2° cells prior to cell pruning (Video 4). When one cell has low-intensity F-actin and increasing area (green arrow), the neighboring cell has high-intensity of F-actin and decreasing area (red arrow). **(E')** Cell area of neighboring 2° LCs is negatively correlated (R = −0.2020 at a peak correlation of +15 s, N = 14 [7 pairs] in three eyes, one-sample t test; P = 0.0318). **(F)** A schematic summarizing the reciprocal coordination of cytoskeletal and mechanical behavior between neighboring LCs. Scale bar = 3 µm.

We found that the AJs were fragmented in Dia^CA-expressing eyes like in MLCK^CA-expressing eyes (Fig. 4 D and Video 5). Dia^CA expression also severely affected cell shape and arrangement in ommatidia (Fig. 4 D). We also observed intercalation defects (yellow arrow) and cavitation of cone cells (white arrows; Fig. 4 D). Unexpectedly, unlike the contraction of LCs in MLCK^CA eyes, Dia^CA expression significantly increased cells' apical area (Fig. 4 E). To determine if Dia^CA affects medioapical actomyosin, we analyzed F-actin organization and behavior in these eyes (Fig. 4 G and Video 5). In WT, F-actin is enriched medioapically and at LC–LC contacts, while in Dia^CA-expressing eyes, it accumulated uniformly in a thick band at the cell periphery and was missing medioapically. It is plausible that by binding efficiently to Rho1 through its RhoGTPase-binding domain, Dia^CA competitively inhibits Rok activation and MyoII phosphorylation, and thus the assembly of the medioapical actomyosin network. Overall, these observations imply that pulsing shape changes caused by medioapical MyoII and F-actin function to maintain force balance in the epithelium, affecting cell shape and arrangement. This further suggests not only that Rho1 levels must be carefully controlled, but also that a balance between network assembly and disassembly is required for epithelial remodeling and integrity.

RhoGEF2 and RhoGAP71E control medioapical actomyosin dynamics
The idea that pulsatile assembly and disassembly of the medioapical actomyosin network is necessary for morphogenesis suggests the importance of upstream regulators. We hypothesized that a Rho1 guanine nucleotide exchange factor (RhoGEF) and a Rho GTPase activating protein (RhoGAP), which respectively activate and deactivate Rho1, could regulate medioapical dynamics (Etienne-Manneville and Hall, 2002; Jaffe and Hall, 2005). To identify these putative regulators, we carried out an RNA interference (RNAi) screen for RhoGEFs and GAPs that influence eye epithelial remodeling. In this screen, we identified *RhoGEF2* and *RhoGAP71E* based on RNAi phenotypes in epithelial remodeling.

RhoGEF2 accelerates the frequency and amplitude of medioapical actomyosin assembly and changes in apical cell area
To study RhoGEF2, we examined RhoGEF2 localization using a RhoGEF2 reporter tagged with GFP (RhoGEF2::GFP) and marked cell outlines using F-actin with Lifeact::Ruby (Mason et al., 2016). RhoGEF2::GFP accumulated medioapically in pulses (Fig. 5 A, yellow arrows) that partially overlapped with medioapical F-actin (green arrowhead). To determine if RhoGEF2 levels correlate with apical cell area, we measured the correlation between RhoGEF2 levels and cell area over time and found a weak negative correlation (Fig. 5 A', left panel), with peak enrichment of RhoGEF2 occurring 15–20 s after peak contraction (Fig. 5 A', right panel, R = −0.1361).

To determine the role of *RhoGEF2* in eye epithelial development, we investigated its effects on epithelial remodeling and actomyosin dynamics. Loss of *RhoGEF2* function in genetically marked mutant cell clones led to severe defects in the arrangement and shape of ommatidia cells (Fig. S4, G–G″). Broad depletion of *RhoGEF2* by RNAi led to weaker defects that included loss of LCs and formation of rosettes that can result from defects in LC intercalation (Fig. S4, E and F). To test if *RhoGEF2* controls medioapical actomyosin dynamics, we examined F-actin and MyoII dynamics in RhoGEF2 RNAi-expressing clones (Fig. 5, B–B‴ and Video 6). We found a decrease in medioapical actomyosin levels in the clones (Fig. 5 B' and Video 6) compared with WT counterparts (Fig. 5 B″, red arrows). There was a weaker peak correlation (at −15 s) between MyoII accumulation and apical cell area contraction in *RhoGEF2* RNAi clones compared with WT counterparts (Fig. 5 B‴). These results provide evidence that RhoGEF2 activates Rho1 to control the assembly of the medioapical actomyosin network and is essential for accurate morphogenesis of the eye.

We also investigated the impact of RhoGEF2 overexpression on these dynamics. We found that RhoGEF2 overexpression induced robust and more frequent changes in the medioapical actomyosin network that coincided with changes in the cell apical area (Fig. 5, C and C'; and Video 6). Actomyosin assembled into a dense network that correlated with apical area contraction (red arrow) and then disassembled (green arrow), resulting in apical area relaxation. The assembly of the medioapical actomyosin network strongly correlated with apical cell area contraction (Fig. 5, C' and D, R = −0.4076 at −15 s) than in WT (Fig. 1 B″ and Fig. S1 B″, R = −0.270 at −15 s). Furthermore, overexpression of RhoGEF2 accelerated F-actin pulse frequency (Fig. 5 C″, 215 ± 56 s) compared with WT (Fig. 5 E, 349 ± 96 s) and enhanced the amplitude of F-actin accumulation (Fig. 5 C‴, 1.9-fold) compared with WT (Fig. 5 F, 1.4-fold). Thus, RhoGEF2 overexpression increased the amplitude and frequency of medioapical actomyosin assembly and phenocopied the Rho1 overexpression phenotypes. Cell recoil velocities in RhoGEF2 expressing cells increased after ablating the medioapical actomyosin network, supporting this conclusion (Fig. S5, C and E; and Fig. S6).

RhoGAP71E promotes the disassembly of the medioapical actomyosin network
To localize RhoGAP71E, we live-imaged a RhoGAP71E reporter tagged with GFP (RhoGAP71E::GFP; Denk-Lobnig et al., 2021). RhoGAP71E::GFP was enriched at the cell surface and subtly accumulated medioapically during cell area contractions (Fig. 6
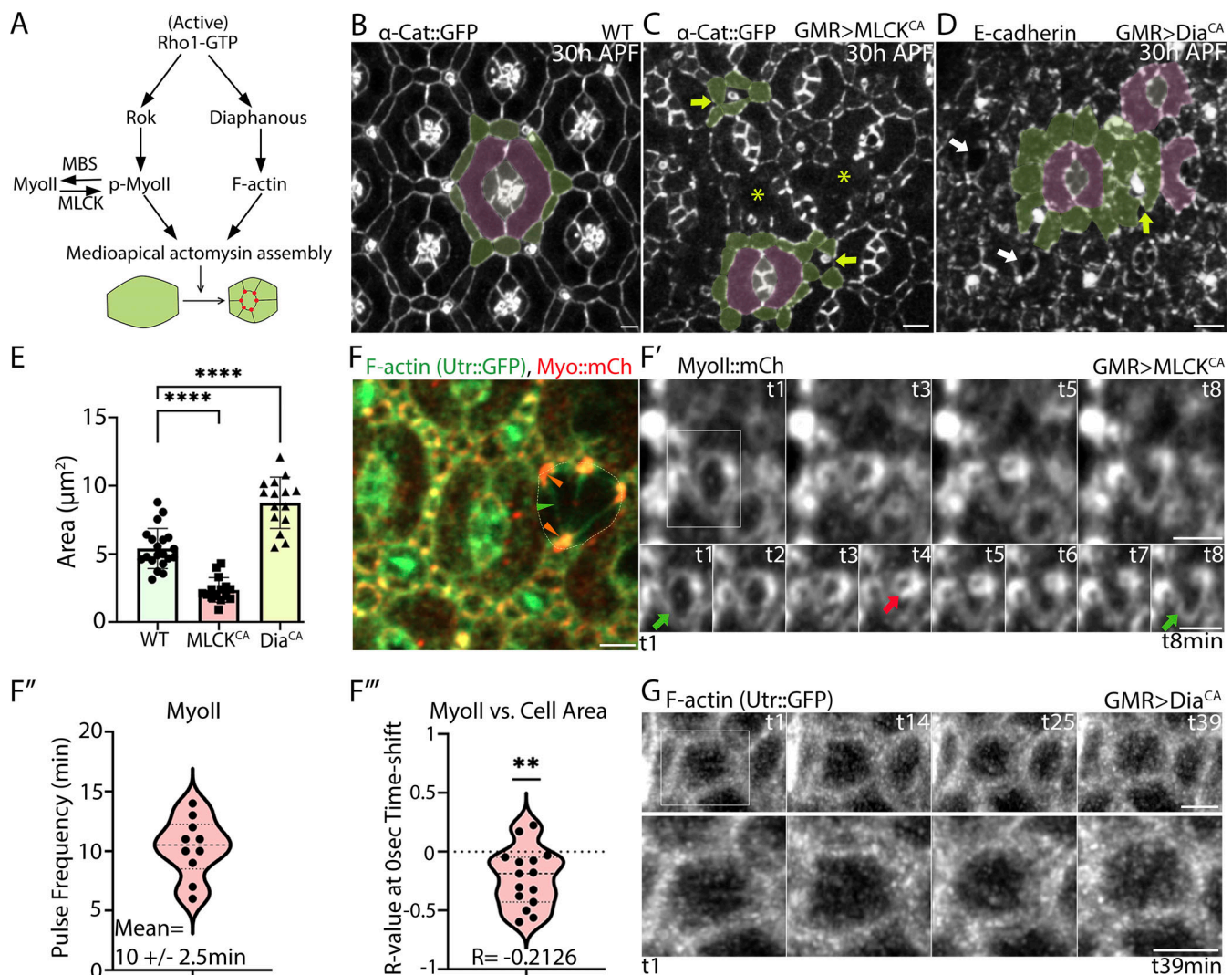
Rosa-Birriel et al.
Biomechanical cell coordination in morphogenesis

Journal of Cell Biology 8 of 19
https://doi.org/10.1083/jcb.202304041

Figure 4. **Turnover of MyoII and F-actin affects medioapical contractile dynamics and is essential for tissue integrity. (A)** Regulation of actomyosin contractility. **(B–D)** Apical cell outlines labeled with α-Cat::GFP in (B) WT, (C) MLCK^{CA}, and (D) Dia^{CA}-expressing eyes. Green and purple overlays highlight LCs and 1° cells, respectively. **(C)** MLCK^{CA} expression results in clustering of LCs around mechanosensory bristles (yellow arrows). The AJs appear fragmented, cells rupture (asterisks), and the planar polarization of ommatidia is disrupted. **(D)** Dia^{CA} expression also results in clustering of LCs (yellow arrow), fragmentation of AJs, and cavitation of cone cells (white arrow). **(E)** MLCK^{CA} expression significantly decreases the apical cell area of 2° LCs, while Dia^{CA} expression increases apical cell area compared with WT. One-way ANOVA with Dunnett's multiple comparisons. WT versus MLCK^{CA} mean R-difference of 3.042, P < 0.0001. WT versus Dia^{CA}, mean R-difference of −3.352, P < 0.0001, N = 20 for WT, 15, and 14, respectively, from three eyes each. **(F)** MLCK^{CA} expression leads to cell rupture. Snapshot from a time-lapse movie (Video 5) of F-actin (Utr::GFP) and MyoII (Sqh::mCh) showing a ruptured cell (marked by the dotted circle) and filamentous actin (green arrowhead) connecting MyoII foci (orange arrowheads) across the rupture. **(F′)** MyoII dynamics in a MLCK^{CA}-expressing eye. A medioapical MyoII ring repeatedly expands (green arrows) and contracts (red arrow). **(F″)** In MLCK^{CA} the frequency of medioapical MyoII ring pulsing is ∼10 min ± 2.5 min (N = 10, 30 pulses in three eyes). **(F‴)** Medioapical MyoII levels are negatively correlated with the apical area of 2° LCs (R = −0.2126, one-sample t test, P = 0.0044, N = 15 in three eyes). **(G)** In Dia^{CA}-expressing eyes, F-actin forms a wide band at the cell periphery and dynamic medioapical F-actin is not present (representative LC from four time-lapse movies). Scale bar = 3 μm.

A, yellow arrow). RhoGAP71E levels peaked 10 s after maximal LC contraction and decreased during apical area expansion (Fig. 6, A–A″, R = −0.1399, blue arrow).

To determine if RhoGAP71E controls medioapical actomyosin dynamics, we first examined the effects of *RhoGAP71E* loss on LCs' remodeling. Eliminating *RhoGAP71E* function or expressing RhoGAP71E RNAi in whole eyes produced flies without eyes. However, using the FLP/FRT (Flippase/Flippase Recognition Target) technique, we were able to recover sparse *RhoGAP71E* mutant cells (Fig. 6 B). The *RhoGAP71E* 1° and 2° mutant cells had

smaller apical areas compared with WT counterparts, suggesting increased actomyosin assembly and tension (Fig. 6 B′). To confirm this, we examined levels of the phosphorylated activated form of MyoII (p-MyoII) in clones expressing RhoGAP71E RNAi (Fig. 6 C). We found an increase in p-MyoII levels in the clones (Fig. 6 C′) compared with WT cells (Fig. 6, C″ and C‴). We also live imaged clones expressing RhoGAP71E RNAi (Fig. 6 D and Video 7). Opposite to the effect of *RhoGEF2* depletion on cell shape, we found a decrease in the apical cell area in cell clones expressing RhoGAP71E RNAi (Fig. 6 D′) compared with WT cells
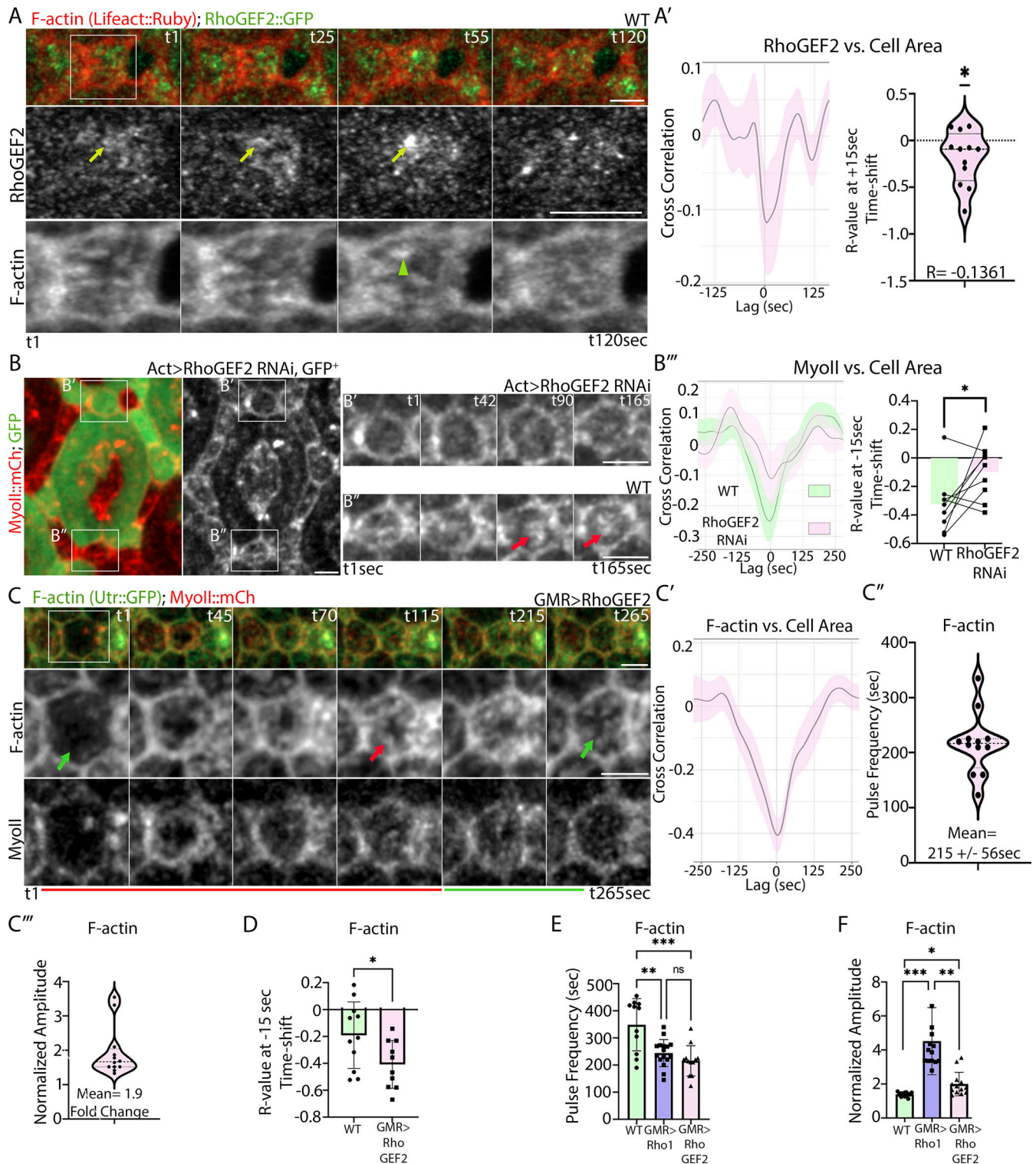
Figure 5. **RhoGEF2 promotes assembly of medioapical actomyosin and apical cell area contraction. (A)** RhoGEF2::GFP and F-actin labeled with Lifeact::Ruby. Snapshots from a time-lapse movie of a lattice edge (top) and magnified views of a 2° LC demarcated with a box. RhoGEF2::GFP (yellow arrow) accumulates medioapically in pulses that correlate with F-actin node enrichment (green arrowhead). **(A')** Left: Time-shifted correlation plot between RhoGEF2::GFP and apical cell area. Right: RhoGEF2::GFP accumulation correlates negatively with cell area at a peak of +15 s (R = −0.1361, N = 12 from three eyes, one-sample *t* test P = 0.0250). **(B–B‴)** Clonal depletion of *RhoGEF2* by RNAi reduces medioapical MyoII assembly compared with the WT counterparts (Video 6). **(B)** Ommatidium with RhoGEF2RNAi-expressing cells (green, upper boxed LC) and WT counterpart (lower boxed LC). **(B' and B")** Time series showing (B') a RhoGEF2RNAi-expressing cell in which MyoII assembly does not occur compared to (B") a WT cell in which MyoII assembles in pulses (red arrow). **(B‴)** Left: Time-shifted correlation plots between medioapical MyoII levels and LC area in RhoGEF2 RNAi-expressing cells (pink) compared with WT (green). Right: Peak correlation is weaker in RhoGEF2 RNAi-expressing cells compared with WT counterparts (paired *t* test, P = 0.0281, N = 8 pairs in four eyes). **(C)** RhoGEF2

overexpression enhances medioapical actomyosin network assembly and apical cell area changes (Video 6). Top: Snapshots of a lattice edge. Bottom: Magnified views of the 2° LC show the assembly (red arrow) and disassembly (green arrow) of the medioapical actomyosin network, corresponding to cell area contraction (red line) and expansion (green line). **(C')** Medioapical F-actin levels correlate with apical area contraction in 2° LCs. **(C" and C''')** Medioapical F-actin pulse frequency is ~3 min (215 ± 56 s, N = 12 from three eyes) in RhoGEF2-overexpressing eyes, with a (C''') 1.9-fold change at their peak than at their trough levels. **(D)** RhoGEF2 expression increases the peak correlation between F-actin and cell area (peak correlation at –15 s, N = 11 from three eyes, t test P = 0.0337). **(E and F)** Rho1 and RhoGEF2 expression increase the frequency and amplitude of F-actin pulses compared with WT. **(E)** Pulse frequencies of medioapical F-actin in WT eyes compared to eyes overexpressing Rho1 and RhoGEF2. One-way ANOVA with Tukey's multiple comparisons. WT versus GMR > Rho1, difference of means = 104 s, P = 0.0010. WT versus GMR > RhoGEF2, difference of means = 133 s, P = 0.0001. GMR > Rho1 versus GMR > RhoGEF2, difference of means = 29 s, P = 0.5084, N = 11, 15, and 16, respectively, from three eyes each. **(F)** Pulse amplitudes of F-actin in the above genotypes. Welch one-way ANOVA with Dunnett's comparison between WT and GMR > Rho1, mean difference of R = –0.3139, P < 0.0001. WT versus GMR > RhoGEF2, mean difference of R = –0.6155, P = 0.0218. GMR > Rho1 versus GMR > RhoGEF2, mean difference of R = 2.523, P = 0.0011, N = 14, 13 and 13, respectively, from three eyes each. Scale bar = 3 μm.

(Fig. 6 D"). The increased assembly of the medioapical actomyosin network in the RhoGAP71E RNAi-expressing cells increased the correlation between MyoII and cell area contraction (Fig. 6 D") and led to increased MyoII pulse frequency compared with WT (Fig. 6 D''', 212 ± 69 s and 387 ± 177 s, respectively), similar to results with RhoGEF2 overexpression. These results indicate that RhoGAP71E inhibits medioapical actomyosin network assembly and thereby regulates the kinetics of pulsing shape changes during LC's remodeling.

We also examined the effects of RhoGAP71E overexpression on medioapical actomyosin and apical cell area fluctuations. RhoGAP71E overexpression expanded the apical cell area and compromised the ability of a subset of cells to hold tension resulting in their expansion (Fig. 6, E–F', asterisk). We also observed a loss of continuity of AJs marked with α-Cat::GFP in highly expanded cells (Fig. 6 F, yellow arrowhead). These results suggest that RhoGAP71E overexpression reduced medioapical tension, allowing the apical cell perimeter to relax. However, we were not able to detect a decrease in cell recoil velocities after ablating the medioapical actomyosin network in RhoGAP71E expressing cells compared with WT (Fig. S5 B). This may reflect compensatory uncoordinated contractions as observed in Rho^{DN} eyes, which may mask the effect in this assay. Although medioapical F-actin fluctuated in these eyes (Fig. 6 G and Video 7), it appeared to be less robust, and network assembly did not correlate with cell area contraction as in WT eyes (Fig. 6 G').

Finally, we examined the interaction between RhoGAP71E and RhoGEF2 by coexpressing the two proteins in the retina. While RhoGAP71E expression alone expanded the apical cell area and led to cell intercalation defects, co-expressing RhoGEF2 with RhoGAP71E suppressed these phenotypes (Fig. S4). Together, these findings provide evidence that RhoGAP71E modulates medioapical actomyosin dynamics and tension by inhibiting Rho1 activity medioapically and antagonizing RhoGEF2 function. Thus, RhoGAP71E and RhoGEF2 regulate the Rho1 GTPase cycle and the overall levels of Rho1 activity to control medioapical actomyosin assembly and contractility, which govern cell shape and arrangement. Moreover, they regulate the kinetics of pulsing shape changes essential for morphogenesis.

The mechanical state of LCs affects Rho1 signaling and actomyosin contractility

To further investigate how cells' mechanical state affects Rho1 activation, we used the Rho1 binding domain of Anillin tagged with GFP (AniRBD::GFP) to visualize the active GTP-bound Rho1 during cell area pulsing (Munjal et al., 2015). In WT cells, this sensor accumulated junctionally and medioapically across the apical cell area and at LC–LC contacts (Fig. 7 A and Video 8). In Rho1-overexpressing retina, this sensor accumulated to high levels and formed aggregates preferentially in LCs (Fig. 7 B). Therefore, we examined the reporter's dynamics relative to cell area fluctuations in cone cells where it minimally aggregated. In WT cone cells, cell contractions and changes in AniRBD were subtle and correlations peaked at –30 s before maximal contraction (Fig. 3 C). In Rho1-overexpressing retina, we found that during the early expansion of cone cells, Rho1 activation was very low in the entire apical region. During mid to late expansion, Rho1 activation gradually increased first at the cell periphery and then also medioapically (Fig. 7 B, right panel, blue and yellow arrowheads, respectively). Finally, during contraction, Rho1 activation continued to increase junctionally and medioapically, concentrating in puncta (blue arrowhead). Although peak correlation was at 10 s after peak contraction, AniRBD began to accumulate before peak expansion. Time correlation analysis revealed a strong correlation with contraction in Rho1-expressing cells (Fig. 7 C). The onset of Rho1 activation during apical area expansion suggests that low tension triggers Rho1 activation to promote contraction and counterbalance cell area expansion.

We also examined the localization of the Rho1 inhibitor RhoGAP71E::GFP in WT and Rho1-overexpressing LCs to determine how the cells' mechanical state relates to the onset of Rho1 inhibition. While in WT eyes, RhoGAP71E::GFP accumulated in pulses that correlated weakly with cell area contraction (Fig. 6, A and A'), in Rho1-overexpressing cells, it accumulated in strong pulses that correlated strongly with cell area contraction (Fig. 7, D and D', red arrowheads and brackets). During cell expansion, RhoGAP71E::GFP accumulated medioapically at low levels (bottom panel, green arrowheads, and brackets), while during late contraction, it accumulated strongly medioapically in punctate structures that then dissipated during early apical area expansion. Strong RhoGAP71E accumulation during apical area contraction suggests that high tension promotes RhoGAP71E recruitment to the apical cell area to inhibit Rho1 and counterbalance contraction.

Overall, our findings show that biochemical and mechanical interactions orchestrate medioapical contractile pulses that shape the *Drosophila* eye. Rho1 activity affects actomyosin contractility and, thereby, the mechanical states of the cells. In turn,
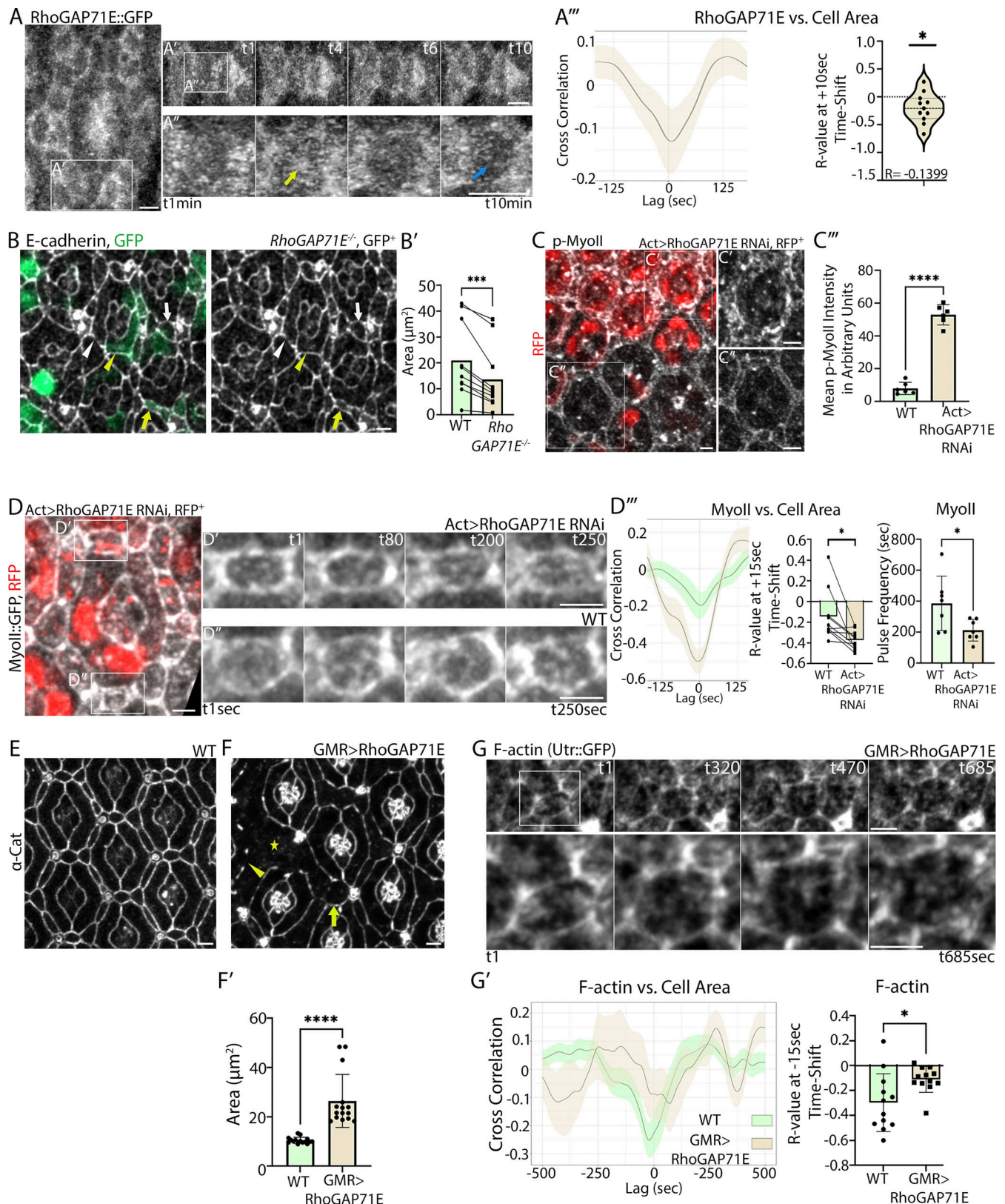
Figure 6. **RhoGAP71E promotes the disassembly of medioapical actomyosin and apical area expansion. (A–A‴)** RhoGAP71E::GFP accumulates medio-apically in pulses. **(A)** Snapshots from a time-lapse movie of an ommatidium. (A′) Lattice edge and (A″) magnified views of a 2° LC demarcated with a box. Note the punctate enrichment of RhoGAP71E at 4 min (yellow arrow) compared with low enrichment at 10 min (blue arrow). **(A‴)** Medioapical RhoGAP71E::GFP levels negatively correlate with apical cell area of 2° LCs at a time shift of +10 s (R = −0.1399, N = 11 from three eyes, one-sample *t* test P = 0.0328). **(B–D)** RhoGAP71E promotes apical cell area expansion. **(B)** *RhoGAP71E* mutant cells positively marked by GFP in fixed tissue stained for E-cadherin. White

arrow, WT LC; yellow arrow, mutant LC; white arrowhead, WT 1° cell; yellow arrowhead, mutant 1° cell. **(B′)** The apical area of the *RhoGAP71E* mutant cells is significantly smaller than that of WT counterparts (connected lines, paired *t* test, P = 0.0007, N = 10 pairs from four eyes). **(C)** RhoGAP71E RNAi expression increases MyoII phosphorylation. **(C′)** p-MyoII levels are higher in RNAi-expressing clones marked with RFP compared with **(C″)** WT regions. **(C‴)** *T* test, P < 0.0001, N = 6 WT and RNAi-expressing clones from three eyes. **(D)** RhoGAP71E RNAi expression decreases apical cell area and strengthens the negative correlation between MyoII accumulation and cell area contraction (Video 7). Left: Snapshot from a time-lapse movie of MyoII (Sqh::GFP) in eyes with Rho-GAP71E RNAi-expressing clones (RFP⁺). **(D′ and D″)** Time series montage of zoomed-in views of (D′) a RhoGAP71E RNAi-expressing 2° LC compared with (D″) a WT counterpart. **(D‴)** Left: Peak correlation (at −15 s) between MyoII accumulation and apical area contraction is higher in RhoGAP71E RNAi-expressing cells (light brown) compared with WT cells (green). Middle: MyoII correlation with cell area contraction is significantly higher in RhoGEF2RNAi-expressing cells than in their WT counterparts (paired *t* test, P = 0.0127, N = 10 pairs from three eyes). Right: RhoGAP71E RNAi expression decreased the time between pulses of MyoII accumulation to ∼3 min (212 ± 69 s) compared with ∼6.5 min in WT (387 ± 177 s, *t* test, P = 0.0109, N = 7 from three eyes). **(E and F)** Compared to (E) WT, (F) RhoGAP71E overexpression causes expansion of the cells' apical area (yellow arrow), and gaps in the continuity of the AJs (yellow arrowheads) in highly expanded cells (asterisk) (Video 7). **(F′)** RhoGAP71E expression significantly increased the apical cell area of 2° LCs compared with WT (N = 14 from three eyes, *t* test, P < 0.0001). **(G)** RhoGAP71E overexpression reduces medioapical F-actin levels. Top: Snapshots of a lattice edge. Bottom: A magnified view of the boxed 2° LC. Lower levels of actomyosin accumulation correlate with shallower fluctuations in the apical cell area. **(G′)** Left: RhoGAP71E overexpression abolishes the correlation between actomyosin accumulation and cell area contraction. Right: Comparison of R-values at a time shift of −15 s between RhoGAP71E-expressing LCs and WT LCs (*t* test, P = 0.0186, N = 12 from three eyes). Scale bar = 3 μm.

Discussion

During epithelial remodeling of the fly retina, at least two dynamic actomyosin networks operate at the apical region of the cells. The first is a junctional network that cyclically contracts and expands the LC–LC contacts (Del Signore et al., 2018; Malin et al., 2022). Here, we describe a second mechanism essential for accurate morphogenesis: a non-ratcheting pulsatile medioapical actomyosin network controlled by Rho1 and its effectors Dia and MyoII. This network is established by flows of F-actin from the cell surface toward the medioapical region where it assembles into actomyosin nodes that generate anisotropic contractile force with the highest force predicting the cell edges that will eventually shorten. This force is transient, and upon release, the actomyosin nodes remodel, disassemble, or merge with the junctional network. Force generated by contractile actomyosin is transmitted between cells, and the loss of force from a neighbor often prompts medioapical actomyosin assembly after initial disassembly and cell area relaxation. More strikingly, pulses of medioapical contraction and release are reciprocally synchronized between adjacent 2° LCs, revealing that these Rho1-regulated networks are integral to biomechanical feedback coupling. That is, they appear to trigger and be triggered by forces between neighboring cells and coordinate their activity. Further supporting this conclusion, we found activation of Rho1 as cells expanded and negative Rho1 regulator RhoGAP71E accumulated as cells contracted. Finally, we note that all manipulations that disrupted the kinetics of medioapical pulsing resulted in developmental errors. These observations expand our understanding of these players' roles in embryonic undifferentiated tissue development to a fully differentiated tissue where they work over different time scales to control cell shape determination.

This is the first investigation of the pulsing features and regulation of medioapical actomyosin networks in retina LCs.

these mechanical states feedback to affect Rho1 signaling (Fig. 7 E). Our discoveries indicate that both molecular and mechanical feedback loops coordinate the mechanical behavior of neighboring cells to rebalance forces in the epithelium and promote tissue remodeling.

Overexpressing Rho1 dramatically revealed that the induced rapid cell area oscillations were inversely coordinated in neighboring 2° LCs: one cell contracted while its neighbor relaxed and vice versa. Although it is known that cells can sense and adapt to mechanical forces (del Rio et al., 2009; Gaertner et al., 2022; Mueller et al., 2017; Spadaro et al., 2017; Yonemura et al., 2010), the current observations expand our understanding of how forces work in this system. Our findings suggest that neighboring LCs and the medioapical actomyosin networks do not merely strike a balance of mechanical forces but are continually adapting to changing forces over time, generating coordinated pulsing changes in cell shape. This is supported by our observation that laser ablation of the medioapical actomyosin network in one cell was often associated with a subsequent actomyosin accumulation and contraction of the neighboring cell following an initial relaxation. More specifically, our results provide evidence that mechanical cell-to-cell interactions can activate or inhibit Rho1 activity and actomyosin contractility and that cells respond to tension and stretching under normal physiological conditions by modulating Rho1 function. Thus, Rho1-dependent medioapical actomyosin networks appear integral to feedback loops that coordinate pulsing in neighboring cells.

Not only was anti-correlated pulsing between neighboring cells detected with Rho1 overexpression, but it was also apparent in WT eyes (Video 1). However, the correlation between actomyosin accumulation and cell area contraction in WT cells had a wide distribution (Fig. S1, B″ and C′). This suggests that the pulsing is highly tuned to work in balance with other ongoing cellular processes that may provide permissive conditions, such as the net force exerted by neighboring cells. The anti-correlated pulsing of neighboring 2° LCs is a unique feature contrasting with other examples of pulsatile contraction. For example, in cell intercalation during germband extension, adjacent cells constrict simultaneously, resulting in loss of contacts and rearrangement of the epithelium (Fernandez-Gonzalez and Zallen, 2011; Rauzi et al., 2010; Sawyer et al., 2011; Vanderleest et al., 2018). In apical constriction, it has been observed that when one cell undergoes ratcheting contraction, ratcheting of nearby cells becomes more likely to stabilize changes in cell shape and facilitate invagination (Xie and Martin, 2015). Likewise, the late phase of dorsal closure involves collective apical area contraction
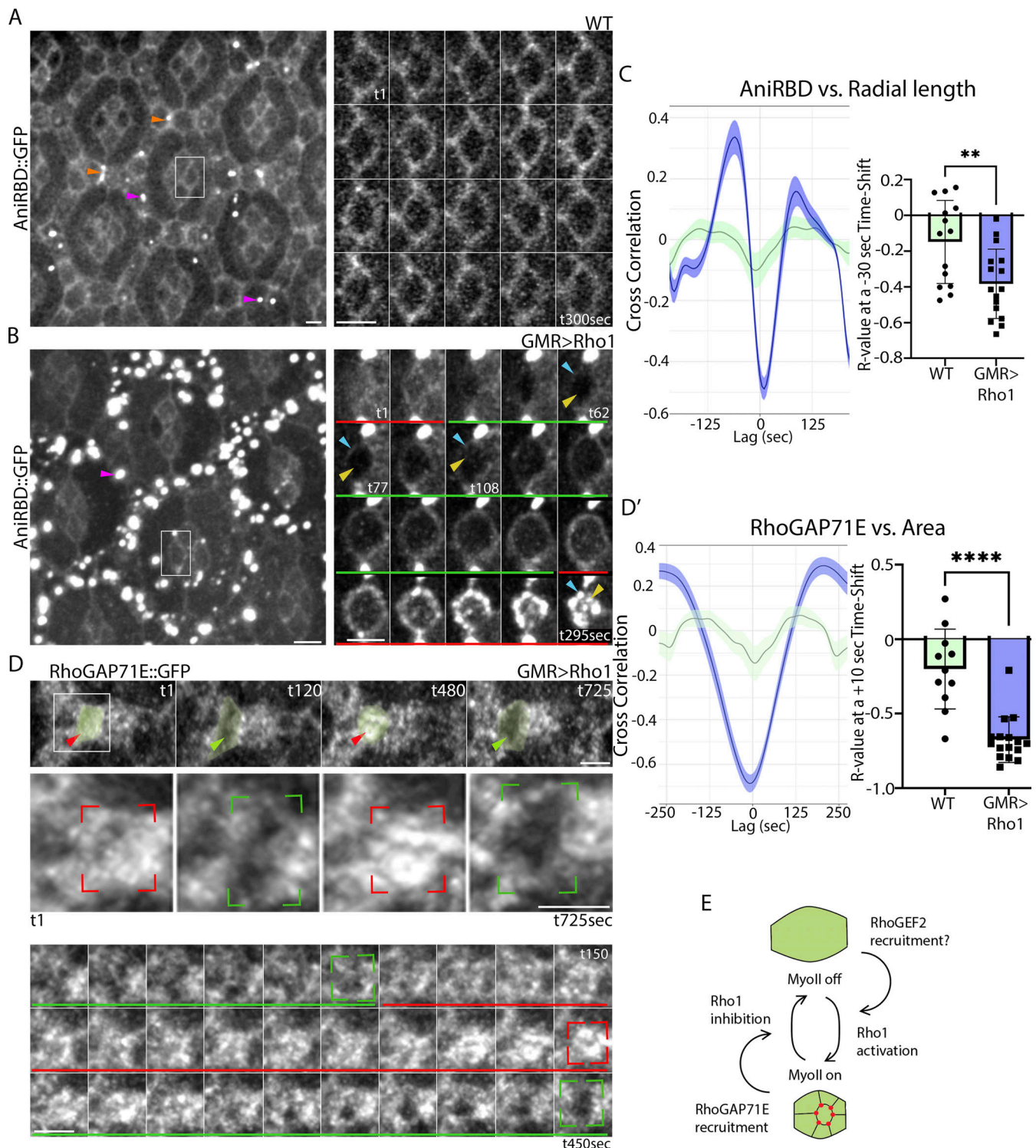
Figure 7. **Cell area expansion triggers Rho1 activation while cell area contraction triggers RhoGAP71E recruitment. (A and B)** Pulses of Rho1 activation in (A) WT and (B) Rho1-expressing eyes were detected using the Rho1 sensor Anillin Rho1 binding domain tagged with GFP (AniRBD::GFP). Left: Snapshots of several ommatidia. Right: Time series montages of (A) WT and (B) Rho1-overexpressing cone cells demarcated by the boxes over a period of 300 s (Video 8). Note widespread high levels of Rho1 activation in Rho1-expressing eyes compared with WT, where there is sporadic enrichment medioapically (purple arrowheads) and in contracting LC–LC contacts (orange arrowheads). **(A)** In WT, cone cells do not expand or contract on this timescale. **(B)** Overexpression of Rho1 induces pulsed expansion and contraction of cone cells. During early cone cell expansion (green lines), levels of Rho1 activation are low at the cell periphery and medioapically (t62; yellow and blue arrowheads, respectively). During mid-expansion Rho1 activation increases first at the cell periphery (t77) and then also in puncta medioapically (t108). As the cells begin to contract (red lines) Rho1 is activated strongly both at the cell periphery and medioapically. **(C)** Overexpressing Rho1 increases the negative correlation of medioapical AniRBD::GFP with cone cell radial length at a time shift of −30 s prior to peak cell expansion, and the correlation continues to rise after peak cell expansion (R = −0.3982, N = 14 for WT, N = 16 for GMR > Rho1 from three eyes each. t test,

P = 0.0063). **(D and D′)** RhoGAP71E accumulates strongly during contraction of LCs in Rho1-overexpressing eyes (Video 8). **(D)** Top: Snapshots of a lattice edge. The 2° LC in the boxed region is highlighted in green. RhoGAP71E::GFP accumulation in contracted cells is indicated with red arrowheads. Low Rho-GAP71E::GFP levels in expanding cells are indicated with green arrowheads. Middle: Zoomed-in images of the 2° LCs (boxed area). The bracketed red zones show medioapical RhoGAP71E::GFP levels increasing with cell area contraction, while bracketed green zones show RhoGAP71E::GFP levels decreasing when cell area expands. Bottom: Longer time series montage of medioapical RhoGAP71E::GFP dynamics over a period of 450 s. RhoGAP71E::GFP levels increase (red bracket) as the cell apical area decreases (red line) and decrease (green brackets) as cell area increases (green lines). **(D′)** A stronger correlation between RhoGAP71E::GFP levels and cell area contraction is observed in GMR > Rho1 compared with WT at a time-shift of +10 s ($N = 11$ in WT and $N = 16$ in GMR > Rho1 from four eyes each, t test, P = 0.0081). **(E)** A cartoon summarizing the cell-autonomous mechanical feedback loops affecting Rho1 activity, actomyosin contractility, and apical cell area. Low tension in expanding cells triggers Rho1 activation to increase tension and promote contraction. High tension in contracting cells triggers the recruitment of RhoGAP71E to inhibit Rho1, decrease tension, and promote expansion. Scale bar = 3 µm.

of amnioserosa cells. In contrast, the early phase exhibits preferential anti-correlated changes in cell shape and medial myosin accumulation in neighboring cells. RhoGEF2 and Rho1 affect these dynamics, with Rho1 acting both autonomously and non-autonomously (Azevedo et al., 2011; Saravanan et al., 2013; Solon et al., 2009), suggesting that the mechanism we discovered may be used in other contexts. Overall, these findings suggest that although Rho1-regulated medioapical actomyosin constriction generally appears sensitive to forces exerted across the epithelium, the cell's specific response to forces imposed by neighbors is a control point with a variable outcome.

Together, these findings indicate that Rho1 dynamics must be tightly controlled in space and time to regulate actomyosin dynamics and epithelial morphogenesis. Using a genetic screen, we identified RhoGEF2 and RhoGAP71E as upstream regulators of Rho1 whose perturbation yielded altered cell shape and arrangement while the integrity of the adherens junctions was maintained. Although we previously identified these genes in a screen for epithelial folding in leg joint morphogenesis and they are both known regulators of Rho1 in other systems, we were surprised to identify these genes because the characteristics of the medioapical actomyosin network in the LCs are unique (Azevedo et al., 2011; Denk-Lobnig et al., 2021; Fox and Peifer, 2007; Greenberg and Hatini, 2011; Häcker and Perrimon, 1998; Mason et al., 2016; Mulinari et al., 2008). In these other cases involving RhoGEF2 and RhoGAP71E, there is typically ratcheting shape change, irreversible loss of contacts, and/or epithelial folding, none of which characterize changes in the retina at this phase of development. Thus, identifying RhoGEF2 and Rho-GAP71E in this study is important because it reveals that their participation is not linked to a particular morphological outcome. Since pulsing appears regulated by forces imposed by neighboring cells, our results also suggest the hypothesis that mechanical forces could, in turn, regulate RhoGEF2 and/or RhoGAP71E. This idea is supported by the observations that Rho1 is activated in expanding cells under low tension and Rho-GAP71E is recruited to the medioapical region in contracting cells under high tension (Fig. 7 E). A related feedback mechanism may control vesicle secretion in *Drosophila* larval salivary glands, where Rho1 initiates actin coat assembly and vesicle contraction. In response, RhoGAP71E accumulates on vesicles and inhibits Rho1, leading to coat disassembly and termination of the contraction cycle (Segal et al., 2018). In sum, these results provide a starting point for the revelation of the regulatory networks that guide these intermediaries to respond to cell's mechanical state.

Furthermore, our data indicate that tuning of pulsing dynamics by Rho1 and its regulators is crucial for the cells to maintain their shape and position in the lattice and prevent catastrophic tissue ruptures during this period of eye development. However, it is interesting to note that with constitutively active MLCK, we continued to observe pulsing accumulation of MyoII, even though the tissue architecture was highly disrupted. This observation is consistent with the idea that a core of pulsing dynamics may arise from the intrinsic biophysical properties of contractile actomyosin networks, wherein as F-actin filaments are exposed to high tension, they spontaneously disassemble (Haviv et al., 2008; Munjal et al., 2015). However, our results would also support the idea that pulsing characteristics are finely tuned to work in balance with other processes occurring in the epithelium to maintain tissue structure and generate the appropriate developmental pattern.

A salient feature of retinal development is the continual movement and shape changes of cells, even though it takes hours for persistent changes to unfold. Our results suggest that continuous cycling of the nucleotide state of the Rho1 GTPases drives Rho1-dependent regulation of the cytoskeleton that underlies components of these movements. Thus, these are active, energy-dependent processes that cells invest in, despite the apparent transience of shape changes seen over the short term. There are various explanations for why medioapical actomyosin pulsing exists in other systems, for example, to enable apical constriction by ratcheting or to utilize the relaxation phase to remove membrane and junctional proteins (Jewett et al., 2017; Miao et al., 2019). Here, in the *Drosophila* retina, it appears medioapical actomyosin pulsing coordinates the mechanical behavior of neighboring cells and functions to maintain mechanical tissue integrity. Previously, we described oscillations of junctional networks of LC–LC contacts that occurred with a periodicity of about 15 min (Del Signore et al., 2018; Malin et al., 2022). Here, pulsing of medioapical actomyosin networks has a periodicity closer to 6 min. While we do not yet know how these processes interplay, it is intriguing to note the existence of multiple sinusoidal functions that could distribute mechanical forces and speculate on how their actions are eventually integrated to generate the precise shaping of the eye.

In summary, we identified a pulsatile medioapical actomyosin network in LCs that exerts tension on the apical cell surface in a pattern that predicts the final shape changes of the cells. This network assembles into a ring of nodes connected by F-actin filaments that exert tension on one another and the cell

surface. RhoGEF2 activates Rho1, actomyosin assembly, and cell area contraction, while RhoGAP71E inhibits Rho1 and promotes actomyosin disassembly and cell area expansion. Low tension in expanding cells triggers Rho1 activation and cell area contraction while rising tension in contracting cells triggers RhoGAP71E recruitment, Rho1 inhibition, and cell area expansion. Contraction of one cell promotes actomyosin disassembly and area expansion of neighboring cells, which in turn triggers Rho1 activation and contraction. Together, these intracellular and cell-to-cell interactions manifest in inversely synchronized cell-to-cell oscillations of actomyosin and apical cell area (Fig. 7 E). Our research suggests that during epithelial remodeling, when the cells are engaged in the pursuit of stable forms, finely tuned pulsing of medioapical actomyosin networks functions in balancing the forces between epithelial cells. Regulated by mechanical and biochemical signals, Rho1 plays a crucial role in this delicate balancing act.

Materials and methods

Fly strains

We employed a RhoGEF2::GFP BAC transgene inserted at the VK33 attP transgene landing site to examine RhoGEF2 dynamics during LCs remodeling (Mason et al., 2016). We expressed UAS-RhoGEF2 protein with an N-terminal T7 tag (RRID:BDSC_9387) to examine the RhoGEF2 overexpression phenotypes, and FRT42D *rhogef2*[e037764] (Kyoto-114511) to generate genetically marked mutant clones. We employed a RhoGAP71E::GFP CRISPR insertion (Denk-Lobnig et al., 2021) and RhoGAP71E::GFP driven by the ubiquitin promoter (this study) to examine RhoGAP71E protein distribution and dynamics, a WT UAS-RhoGAP71E (this study) to examine overexpression phenotypes, and *RhoGAP71E*[j6B9] FRT80B (Kyoto-111395) to generate genetically marked mutant clones.

Fly lines from the Bloomington *Drosophila* Stock Center: (1) Rho1::GFP (RRID:BDSC_9528), (2) UAS-Rho1.N19 (RRID:BDSC_58818), (3) UAS-Rho1 (RRID:BDSC_28872), (4) UAS-MLCK.Ct (RRID:BDSC_37527, 37528), (5) UAS-Dia.CA (RRID:BDSC_27616), (6) UAS-T7.RhoGEF2 (RRID:BDSC_9387), (7) UAS-Lifeact::Ruby (RRID:BDSC_35545), (8) sqh-GFP::Rok (RRID:BDSC_52289), (9) GMR-GAL4 (RRID:BDSC_9146, 84247), (10) *y w*; Actin>y+>GAL4, UAS-GFP (RRID:BDSC_4411), (11) *w*; Actin>CD2stop>GAL4, UAS-mRFP (RRID:BDSC_30558), (12) *y w*; α-Cat::GFP[gfstf] (RRID:BDSC_59405), (13) *y w* hsFLP; UAS-GFP[nls] (RRID:BDSC_9431), (14) *w*; tub-GAL4; FRT40A, tub-GAL80[ts] (RRID:BDSC_86315), (15) *w*; FRT80B, Ubi-GFP (RRID:BDSC_1620), (17) UAS-RhoGEF2-RNAi (RRID:BDSC_34643), and (18) UAS-RhoGAP71E-RNAi (RRID:BDSC_32417). α-Cat::Venus[CPTI002596] (115551) and *RhoGAP71E*[j6B9] FRT80B (111395) and FRT42D *RhoGEF2*[e037764] (114511) were obtained from the Kyoto Stock Center. Fly lines generated in the lab for Del Signore et al. (2018) and Malin et al. (2022): (1) UAS-Lifeact::Ruby; GMR-GAL4, (2) UAS-Lifeact::GFP; Sqh-Sqh::mCherry, GMR-GAL4, and (3) UAS-Lifeact::Ruby; Sqh-Rok::GFP, GMR-GAL4. Additional stocks used: (1) Sqh-Sqh::mCherry, (2) Sqh-UtrABD::GFP, Sqh-Sqh::mCherry (Martin et al., 2009), (3) GMR-GAL4, UAS–α-Cat::GFP (Larson et al., 2008), (4) RhoGAP71E::GFP (Mason et al., 2016), (5) RhoGEF::GFP (Mason et al., 2016), and (6) AniRBD::GFP (Munjal et al., 2015).

Molecular biology and construction of genetically encoded reporters

We generated several new reporters driven by the UAS and the ubiquitin promoter, including Ubi-RhoGAP71E::GFP and UAS-RhoGAP71E::GFP. The *RhoGAP71E* open reading frame (ORF) was amplified from cDNA clone LD04071. The PCR products were inserted into the pENTR plasmid by Topo cloning. All expression clones were generated by the Gateway technology using the *Drosophila* Gateway Vector Collections (obtained from the *Drosophila* Genomics Resource Center) using the Clonase II reaction to fuse the ORFs in frame with a desired fluorescent protein. Transgenic flies carrying these transgenes were established by standard methods by BestGene, Inc.

Genetic analysis

GMR-GAL4 was used to broadly express UAS-transgenes in the eye (Wernet et al., 2003). The FLP/FRT (Xu and Rubin, 1993) and Mosaic Analysis with a Repressible Cell Marker techniques (Lee and Luo, 2001) were used to generate genetically marked clones by FLP-mediated mitotic recombination and the FLP-Out/GAL4 technique to express desired transgenes in genetically marked clones. hsFLP; Ubi-GFP, FRT80B was used to generate *RhoGAP71E* mutant FLP/FRT clones, and hsFLP; FRT42D Ubi-GFP was used to generate the *RhoGEF2* mutant clones. Mitotic and FLP-Out clones were induced by a heat shock for 30 min at 34°C.

Method details

Immunofluorescence

White prepupae (0 h after puparium formation or APF) were selected and aged on glass slides in a humidifying chamber at 25°C. Pupal eyes were dissected in phosphate-buffered saline (PBS), fixed for 35 min in 4% paraformaldehyde in PBS, and stained with antibodies in PBS with 3% BSA, 0.3% Triton X-100, and 0.01% sodium azide. Primary antibodies used were rat anti-E-cad (1:100, #DCAD2; DSHB), mouse anti-Dlg (1:500, #4F3; DSHB), and guinea pig anti-Sqh1P (Zhang and Ward, 2011). The following ThermoFisher conjugated secondary antibodies were used at 1:150: Alexa 405 (RRID:AB_221604), Alexa488 (RRID:AB_143165, AB_2534069), and Alexa647 (RRID:AB_2535805). The following Jackson ImmunoReaserch conjugated secondary antibodies were used at 1:150: Cy3 (RRID: AB_2632516, AB_2632516) and Cy5 (RRID: AB_2338713, AB_2338713).

Confocal time-lapse imaging

Flies were selected for imaging at 0 h APF and aged at 25°C unless described otherwise. Pupae were mounted in a slit created in an agarose block with eyes facing the coverslip after the operculum for each pupa was removed. The agarose block was surrounded by a Sylgard 184 gasket prepared in the lab and capped with a custom-built humidified chamber. Time-lapse imaging was performed on a Zeiss LSM800 inverted laser scanning confocal microscope with Airyscan. Images were taken every 5, 30, and 60 s as noted with an optimal pinhole (1 AU) using a 63×, 1.4-NA, plan Apochromat immersion objective, 0.7 µm per optical section with a 10–50% overlap between sections, at a scan speed of 6–7 with no averaging in Zeiss Zen Blue 2.6 software.

Laser ablation

Laser nano-ablations to probe tissue mechanics were performed using a Zeiss LSM880 NLO with a near-infrared InSight X3 two-photon tunable laser (680–1,300 nm) using a 740 nm multi-photon excitation. Samples were imaged with Utr::GFP and Sqh::mCh to identify the medioapical actomyosin network for ablation using a 63× oil immersion objective (NA 1.4). A small field size of 4 × 4 pixels was ablated in the center of either 2° or 3° LCs using a 30–40% laser output, at a scan speed of one, with one iteration. Images were collected every second for 250 s in a frame of 1,584 × 1,584 pixels to calculate cell recoil velocity or for 10 min to examine cell-to-cell mechanical interactions in Zeiss Zen Black 2.3 software. Ablations were performed 6 s after the beginning of each experiment.

Quantification and statistical analyses
Cell expansion analysis

The areas of 2° and 3° LCs were measured in Fiji immediately before and 180 s after ablation to calculate the fold expansion of the apical cell area. Ratios were calculated in Microsoft Excel by dividing the area after ablation by the area before ablation. LC–LC (2°-3°), 2°-1°, and 3°-1 contact lengths for both 2° and 3° LCs were also measured before ablation and 180 s after ablation. Ratios were plotted in GraphPad Prism 9 and compared with normalized contact length before ablation.

Correlation analysis between apical cell area and the signal intensity of fluorescent reporters and initial recoil velocity measurements

We measured the mean signal intensity of F-actin (using Utr::GFP), MyoII (using MyoII::mCh), RhoGEF2::GFP, RhoGAP71E::GFP, and apical cell area at 28 h APF in time-lapse movies with a time resolution of 5 s. Using the Fiji polygon selection tool, we manually traced individual apical perimeters of 2° LCs. Regions of interest (ROIs) were generated, and minimum, maximum, and mean average signal intensities were obtained for each cell and normalized against the background. Using a custom R script, we measured the time-shifted Pearson's cross-correlations (time windows from ±8 min) between the mean signal intensities of the fluorescent reporter and cell area using 20–30-min-long movies. The data were smoothed using an "R" kernel regression smoother and presented as the average Pearson's correlation of individual cells and the standard error of the mean. A one-sample t test was performed on the average changes in R-values for apical cell area versus RhoGEF2::GFP, apical cell area versus RhoGAP71E::GFP, apical cell area versus Utr::GFP, apical cell area versus Sqh::mCh, and apical cell area versus MyoII in Act>RhoGAP71E RNAi- and Act>RhoGEF2 RNAi-expressing cells with a theoretical mean of 0. Pulse duration was obtained after plotting the apical cell area against time. Distances between the maxima were obtained and averaged. Amplitudes were obtained by calculating the distance between the maxima and minima to obtain an average amplitude or fold-change of signal intensity. For the cell-to-cell comparisons, R-values were generated for the correlation between areas of adjacent 2° LCs and between the area of one cell and actin intensity in the neighboring cell. R-values were averaged and a

one-sample t test was performed against a theoretical mean of 0. To calculate the initial area recoil velocity (V_0), we measured the area of the 2° LCs after ablation for a period of 60 s in Fiji, which changed linearly during this time interval. Subsequently, we plotted the area against time in GraphPad Prism 9 and computed the V_0 by averaging the slopes of the fitted lines.

Comparing signal intensities between WT and RNAi-expressing cell clones

LCs were selected for analysis if all adjacent cells expressed the RNAi, or, for the control group, if all adjacent cells were WT. For each 2° LCs, circular ROIs were used to measure the signal intensity at the medioapical region from which the background was subtracted to calculate the average signal intensity in RhoGAP71E RNAi or RhoGEF2 RNAi compared with WT LCs. A t test for normally distributed data and a Mann–Whitney test for non-normally distributed data were used to compare the groups.

Online supplemental material

Fig. S1 shows medioapical actomyosin network assembly imaged at a high spatial and temporal resolution that negatively correlates with cell area changes. Fig. S2 shows the reassembly of medioapical F-actin network after ablation. Fig. S3 shows negatively correlated cytoskeletal and mechanical coupling between anterior and posterior cone cells and 1° cells. Fig. S4 shows that RhoGEF2 overexpression rescues cell shape and rearrangement defects induced by RhoGAP71E overexpression and RhoGEF2 RNAi and clonal phenotypes. Fig. S5 shows the recoil velocity of 2° LCs that overexpress RhoGAP71E, RhoGEF2, and Rho1 compared with WT. Fig. S6 shows that ablation of medioapical actomyosin in 2° LCs preferentially expands LC–LC contacts, while ablation in 3° LCs preferentially expands 3°-1° contacts. Video 1 shows medioapical F-actin network dynamics in WT LCs with nodes forming a ring and then fusing or remodeling. Video 2 shows anisometric apical area relaxation of 2° and 3° LCs after laser ablation of their medioapical actomyosin network. Video 3 shows that Rho1 overexpression accelerates medioapical F-actin dynamics and cell area fluctuations of LCs compared with WT. Video 4 shows that medioapical actomyosin network assembly and cell area fluctuations are inversely coordinated between neighboring 2° LCs. Video 5 shows that constitutive F-actin and MyoII assembly disrupt medioapical actomyosin organization and dynamics. Video 6 shows that RhoGEF2 promotes medioapical F-actin and MyoII dynamics in LCs. Video 7 shows that RhoGAP71E inhibits medioapical F-actin and MyoII dynamics in LCs. Video 8 shows that in Rho1-expressing eyes, Rho1 is initially activated in expanding cells through the use of the AniRBD::GFP Rho1 sensor, whereas the Rho1 inhibitor Rho-GAP71E tagged with GFP (RhoGAP71E::GFP) accumulates in contracting cells.

Data availability

All data needed to evaluate the conclusions in the paper are present in the article and/or the supplementary materials. Key image data were deposited in the Tufts University Dataverse with the DOI https://doi.org/10.7910/DVN/LGL8PS. Image data and other supporting data of this study are available from the

corresponding author upon reasonable request. Requests for reagents should be directed to and will be fulfilled by the lead contact, Victor Hatini (victor.hatini@tufts.edu).

References

Abreu-Blanco, M.T., J.M. Verboon, R. Liu, J.J. Watts, and S.M. Parkhurst. 2012. Drosophila embryos close epithelial wounds using a combination of cellular protrusions and an actomyosin purse string. *J. Cell Sci.* 125: 5984–5997. https://doi.org/10.1242/jcs.109066

Azevedo, D., M. Antunes, S. Prag, X. Ma, U. Hacker, G.W. Brodland, M.S. Hutson, J. Solon, and A. Jacinto. 2011. DRhoGEF2 regulates cellular tension and cell pulsations in the Amnioserosa during *Drosophila* dorsal closure. *PLoS One.* 6:e23964. https://doi.org/10.1371/journal.pone.0023964

Bao, S., and R. Cagan. 2005. Preferential adhesion mediated by Hibris and Roughest regulates morphogenesis and patterning in the *Drosophila* eye. *Dev. Cell.* 8:925–935. https://doi.org/10.1016/j.devcel.2005.03.011

Bao, S., K.F. Fischbach, V. Corbin, and R.L. Cagan. 2010. Preferential adhesion maintains separation of ommatidia in the *Drosophila* eye. *Dev. Biol.* 344: 948–956. https://doi.org/10.1016/j.ydbio.2010.06.013

Blackie, L., M. Tozluoglu, M. Trylinski, R.F. Walther, F. Schweisguth, Y. Mao, and F. Pichaud. 2021. A combination of Notch signaling, preferential adhesion and endocytosis induces a slow mode of cell intercalation in the *Drosophila* retina. *Development.* 148:148. https://doi.org/10.1242/dev.197301

Blackie, L., R.F. Walther, M.F. Staddon, S. Banerjee, and F. Pichaud. 2020. Cell-type-specific mechanical response and myosin dynamics during retinal lens development in *Drosophila*. *Mol. Biol. Cell.* 31:1355–1369. https://doi.org/10.1091/mbc.E19-09-0523

Blanchard, G.B., S. Murugesu, R.J. Adams, A. Martinez-Arias, and N. Gorfinkiel. 2010. Cytoskeletal dynamics and supracellular organisation of

cell shape fluctuations during dorsal closure. *Development.* 137: 2743–2752. https://doi.org/10.1242/dev.045872

Cagan, R. 2009. Principles of *Drosophila* eye differentiation. *Curr. Top. Dev. Biol.* 89:115–135. https://doi.org/10.1016/S0070-2153(09)89005-4

Cagan, R.L., and D.F. Ready. 1989. The emergence of order in the *Drosophila* pupal retina. *Dev. Biol.* 136:346–362. https://doi.org/10.1016/0012-1606(89)90261-3

Carthew, R.W. 2007. Pattern formation in the *Drosophila* eye. *Curr. Opin. Genet. Dev.* 17:309–313. https://doi.org/10.1016/j.gde.2007.05.001

Dawes-Hoang, R.E., K.M. Parmar, A.E. Christiansen, C.B. Phelps, A.H. Brand, and E.F. Wieschaus. 2005. Folded gastrulation, cell shape change and the control of myosin localization. *Development.* 132:4165–4178. https://doi.org/10.1242/dev.01938

del Rio, A., R. Perez-Jimenez, R. Liu, P. Roca-Cusachs, J.M. Fernandez, and M.P. Sheetz. 2009. Stretching single talin rod molecules activates vinculin binding. *Science.* 323:638–641. https://doi.org/10.1126/science.1162912

Del Signore, S.J., R. Cilla, and V. Hatini. 2018. The WAVE regulatory complex and branched F-actin counterbalance contractile force to control cell shape and packing in the *Drosophila* eye. *Dev. Cell.* 44:471–483.e4. https://doi.org/10.1016/j.devcel.2017.12.025

Denk-Lobnig, M., J.F. Totz, N.C. Heer, J. Dunkel, and A.C. Martin. 2021. Combinatorial patterns of graded RhoA activation and uniform F-actin depletion promote tissue curvature. *Development.* 148:148. https://doi.org/10.1242/dev.199232

Etienne-Manneville, S., and A. Hall. 2002. Rho GTPases in cell biology. *Nature.* 420:629–635. https://doi.org/10.1038/nature01148

Fernandez-Gonzalez, R., and J.A. Zallen. 2011. Oscillatory behaviors and hierarchical assembly of contractile structures in intercalating cells. *Phys. Biol.* 8:045005. https://doi.org/10.1088/1478-3975/8/4/045005

Fox, D.T., and M. Peifer. 2007. Abelson kinase (Abl) and RhoGEF2 regulate actin organization during cell constriction in *Drosophila*. *Development.* 134:567–578. https://doi.org/10.1242/dev.02748

Gaertner, F., P. Reis-Rodrigues, I. de Vries, M. Hons, J. Aguilera, M. Riedl, A. Leithner, S. Tasciyan, A. Kopf, J. Merrin, et al. 2022. WASp triggers mechanosensitive actin patches to facilitate immune cell migration in dense tissues. *Dev. Cell.* 57:47–62.e9. https://doi.org/10.1016/j.devcel.2021.11.024

Greenberg, L., and V. Hatini. 2011. Systematic expression and loss-of-function analysis defines spatially restricted requirements for *Drosophila* RhoGEFs and RhoGAPs in leg morphogenesis. *Mech. Dev.* 128:5–17. https://doi.org/10.1016/j.mod.2010.09.001

Häcker, U., and N. Perrimon. 1998. DRhoGEF2 encodes a member of the Dbl family of oncogenes and controls cell shape changes during gastrulation in *Drosophila*. *Genes Dev.* 12:274–284. https://doi.org/10.1101/gad.12.2.274

Haviv, L., D. Gillo, F. Backouche, and A. Bernheim-Groswasser. 2008. A cytoskeletal demolition worker: Myosin II acts as an actin depolymerization agent. *J. Mol. Biol.* 375:325–330. https://doi.org/10.1016/j.jmb.2007.09.066

Hayashi, T., and R.W. Carthew. 2004. Surface mechanics mediate pattern formation in the developing retina. *Nature.* 431:647–652. https://doi.org/10.1038/nature02952

Jaffe, A.B., and A. Hall. 2005. Rho GTPases: Biochemistry and biology. *Annu. Rev. Cell Dev. Biol.* 21:247–269. https://doi.org/10.1146/annurev.cellbio.21.020604.150721

Jewett, C.E., T.E. Vanderleest, H. Miao, Y. Xie, R. Madhu, D. Loerke, and J.T. Blankenship. 2017. Planar polarized Rab35 functions as an oscillatory ratchet during cell intercalation in the *Drosophila* epithelium. *Nat. Commun.* 8:476. https://doi.org/10.1038/s41467-017-00553-0

Johnson, R.I. 2021. Hexagonal patterning of the *Drosophila* eye. *Dev. Biol.* 478: 173–182. https://doi.org/10.1016/j.ydbio.2021.07.004

Johnson, R.I., M.J. Seppa, and R.L. Cagan. 2008. The *Drosophila* CD2AP/CIN85 orthologue Cindr regulates junctions and cytoskeleton dynamics during tissue patterning. *J. Cell Biol.* 180:1191–1204. https://doi.org/10.1083/jcb.200706108

Larson, D.E., Z. Liberman, and R.L. Cagan. 2008. Cellular behavior in the developing *Drosophila* pupal retina. *Mech. Dev.* 125:223–232. https://doi.org/10.1016/j.mod.2007.11.007

Lee, T., and L. Luo. 2001. Mosaic analysis with a repressible cell marker (MARCM) for *Drosophila* neural development. *Trends Neurosci.* 24: 251–254. https://doi.org/10.1016/S0166-2236(00)01791-4

Letizia, A., D. He, S. Astigarraga, J. Colombelli, V. Hatini, M. Llimargas, and J.E. Treisman. 2019. Sidekick is a key component of tricellular adherens junctions that acts to resolve cell rearrangements. *Dev. Cell.* 50: 313–326.e5. https://doi.org/10.1016/j.devcel.2019.07.007

Magie, C.R., M.R. Meyer, M.S. Gorsuch, and S.M. Parkhurst. 1999. Mutations in the Rho1 small GTPase disrupt morphogenesis and segmentation during early *Drosophila* development. *Development*. 126:5353–5364. https://doi.org/10.1242/dev.126.23.5353

Malin, J., C. Rosa Birriel, S. Astigarraga, J.E. Treisman, and V. Hatini. 2022. Sidekick dynamically rebalances contractile and protrusive forces to control tissue morphogenesis. *J. Cell Biol.* 221:e202107035. https://doi.org/10.1083/jcb.202107035

Martin, A.C., M. Kaschube, and E.F. Wieschaus. 2009. Pulsed contractions of an actin-myosin network drive apical constriction. *Nature.* 457:495–499. https://doi.org/10.1038/nature07522

Martin, P., and J. Lewis. 1992. Actin cables and epidermal movement in embryonic wound healing. *Nature.* 360:179–183. https://doi.org/10.1038/360179a0

Mason, F.M., S. Xie, C.G. Vasquez, M. Tworoger, and A.C. Martin. 2016. RhoA GTPase inhibition organizes contraction during epithelial morphogenesis. *J. Cell Biol.* 214:603–617. https://doi.org/10.1083/jcb.201603077

Miao, H., T.E. Vanderleest, C.E. Jewett, D. Loerke, and J.T. Blankenship. 2019. Cell ratcheting through the Sbf RabGEF directs force balancing and stepped apical constriction. *J. Cell Biol.* 218:3845–3860. https://doi.org/10.1083/jcb.201905082

Mizuno, T., M. Amano, K. Kaibuchi, and Y. Nishida. 1999. Identification and characterization of *Drosophila* homolog of Rho-kinase. *Gene.* 238: 437–444. https://doi.org/10.1016/S0378-1119(99)00351-0

Mueller, J., G. Szep, M. Nemethova, I. de Vries, A.D. Lieber, C. Winkler, K. Kruse, J.V. Small, C. Schmeiser, K. Keren, et al. 2017. Load adaptation of lamellipodial actin networks. *Cell.* 171:188–200.e16. https://doi.org/10.1016/j.cell.2017.07.051

Mulinari, S., M.P. Barmchi, and U. Häcker. 2008. DRhoGEF2 and diaphanous regulate contractile force during segmental groove morphogenesis in the *Drosophila* embryo. *Mol. Biol. Cell.* 19:1883–1892. https://doi.org/10.1091/mbc.e07-12-1230

Munjal, A., J.M. Philippe, E. Munro, and T. Lecuit. 2015. A self-organized biomechanical network drives shape changes during tissue morphogenesis. *Nature.* 524:351–355. https://doi.org/10.1038/nature14603

Rauzi, M., P.F. Lenne, and T. Lecuit. 2010. Planar polarized actomyosin contractile flows control epithelial junction remodelling. *Nature.* 468: 1110–1114. https://doi.org/10.1038/nature09566

Saravanan, S., C. Meghana, and M. Narasimha. 2013. Local, cell-nonautonomous feedback regulation of myosin dynamics patterns transitions in cell behavior: A role for tension and geometry? *Mol. Biol. Cell.* 24:2350–2361. https://doi.org/10.1091/mbc.e12-12-0868

Sawyer, J.K., W. Choi, K.C. Jung, L. He, N.J. Harris, and M. Peifer. 2011. A contractile actomyosin network linked to adherens junctions by Canoe/afadin helps drive convergent extension. *Mol. Biol. Cell.* 22:2491–2508. https://doi.org/10.1091/mbc.e11-05-0411

Segal, D., A. Zaritsky, E.D. Schejter, and B.Z. Shilo. 2018. Feedback inhibition of actin on Rho mediates content release from large secretory vesicles. *J. Cell Biol.* 217:1815–1826. https://doi.org/10.1083/jcb.201711006

Seppa, M.J., R.I. Johnson, S. Bao, and R.L. Cagan. 2008. Polychaetoid controls patterning by modulating adhesion in the *Drosophila* pupal retina. *Dev. Biol.* 318:1–16. https://doi.org/10.1016/j.ydbio.2008.02.022

Solon, J., A. Kaya-Copur, J. Colombelli, and D. Brunner. 2009. Pulsed forces timed by a ratchet-like mechanism drive directed tissue movement during dorsal closure. *Cell.* 137:1331–1342. https://doi.org/10.1016/j.cell.2009.03.050

Spadaro, D., S. Le, T. Laroche, I. Mean, L. Jond, J. Yan, and S. Citi. 2017. Tension-dependent stretching activates ZO-1 to control the junctional localization of its interactors. *Curr. Biol.* 27:3783–3795.e8. https://doi.org/10.1016/j.cub.2017.11.014

Vanderleest, T.E., C.M. Smits, Y. Xie, C.E. Jewett, J.T. Blankenship, and D. Loerke. 2018. Vertex sliding drives intercalation by radial coupling of adhesion and actomyosin networks during *Drosophila* germband extension. *Elife.* 7:e34586. https://doi.org/10.7554/eLife.34586

Warner, S.J., and G.D. Longmore. 2009a. Cdc42 antagonizes Rho1 activity at adherens junctions to limit epithelial cell apical tension. *J. Cell Biol.* 187: 119–133. https://doi.org/10.1083/jcb.200906047

Warner, S.J., and G.D. Longmore. 2009b. Distinct functions for Rho1 in maintaining adherens junctions and apical tension in remodeling epithelia. *J. Cell Biol.* 185:1111–1125. https://doi.org/10.1083/jcb.200901029

Wernet, M.F., T. Labhart, F. Baumann, E.O. Mazzoni, F. Pichaud, and C. Desplan. 2003. Homothorax switches function of *Drosophila* photoreceptors from color to polarized light sensors. *Cell.* 115:267–279. https://doi.org/10.1016/S0092-8674(03)00848-1

Wood, W., A. Jacinto, R. Grose, S. Woolner, J. Gale, C. Wilson, and P. Martin. 2002. Wound healing recapitulates morphogenesis in *Drosophila* embryos. *Nat. Cell Biol.* 4:907–912. https://doi.org/10.1038/ncb875

Xie, S., and A.C. Martin. 2015. Intracellular signalling and intercellular coupling coordinate heterogeneous contractile events to facilitate tissue folding. *Nat. Commun.* 6:7161. https://doi.org/10.1038/ncomms8161

Xu, T., and G.M. Rubin. 1993. Analysis of genetic mosaics in developing and adult Drosophila tissues. *Development.* 117:1223–1237. https://doi.org/10.1242/dev.117.4.1223

Yonemura, S., Y. Wada, T. Watanabe, A. Nagafuchi, and M. Shibata. 2010. alpha-Catenin as a tension transducer that induces adherens junction development. *Nat. Cell Biol.* 12:533–542. https://doi.org/10.1038/ncb2055

Zhang, L., and R.E. Ward IV. 2011. Distinct tissue distributions and subcellular localizations of differently phosphorylated forms of the myosin regulatory light chain in *Drosophila*. *Gene Expr. Patterns.* 11:93–104. https://doi.org/10.1016/j.gep.2010.09.008
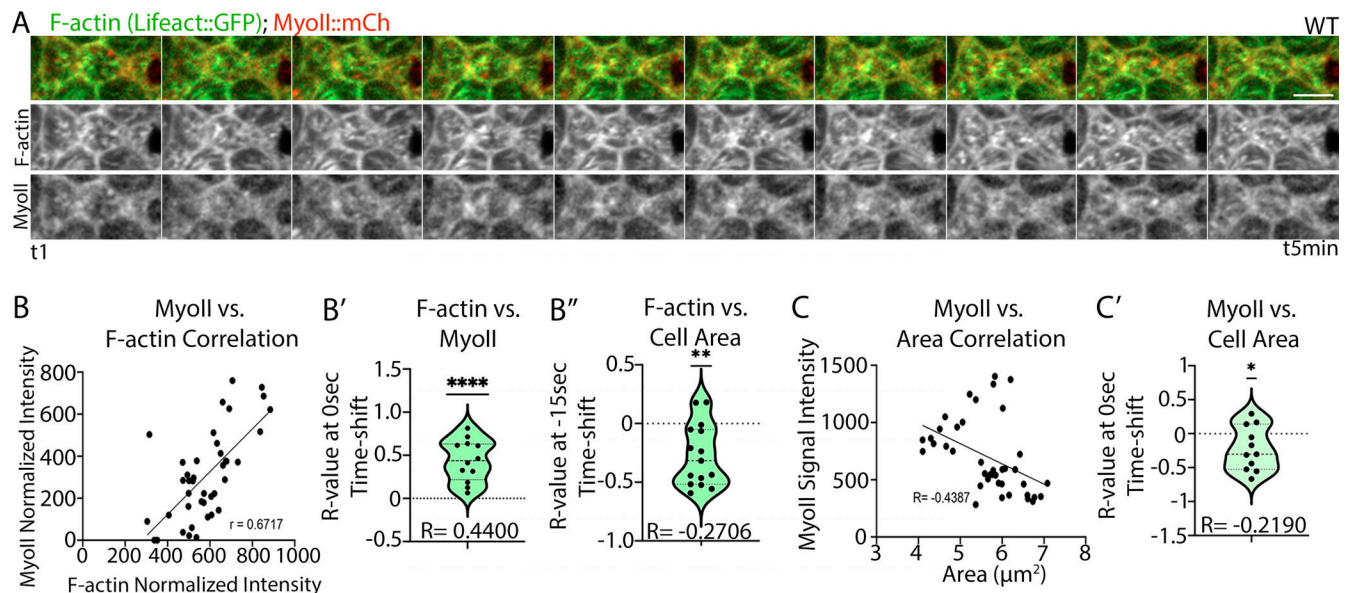
Figure S1. **Pulsatile medioapical actomyosin network assembly correlates with apical cell area contractions. (A)** High-resolution Airyscan time-lapse movie of F-actin (Lifeact::GFP) and MyoII (MyoII::mCh) taken every 30 s. Note F-actin and MyoII accumulation in nodes and filamentous structures. **(B)** Positive Pearson's correlation between F-actin and MyoII in a single LC. **(B')** Time-shifted Pearson's correlation between medioapical F-actin and MyoII shows a strong positive correlation at 0 s time-shift (mean R = 0.4400, N = 15 cells from three eyes, one-sample t test: P < 0.0001). **(B")** Time-shifted Pearson's correlation between medioapical F-actin and apical cell area shows a negative correlation at a −15 s time-shift (mean R = −0.2706, N = 15 cells from three eyes, one-sample t test: P = 0.0014). **(C)** Negative Pearson's correlation between MyoII intensity and apical cell area in a single LC. **(C')** One sample t test shows a significant negative correlation between medioapical MyoII levels and cell area at a 0 s time-shift (mean R = −0.2190, N = 11 from three eyes, P = 0.0482). Scale bar = 3 μm.
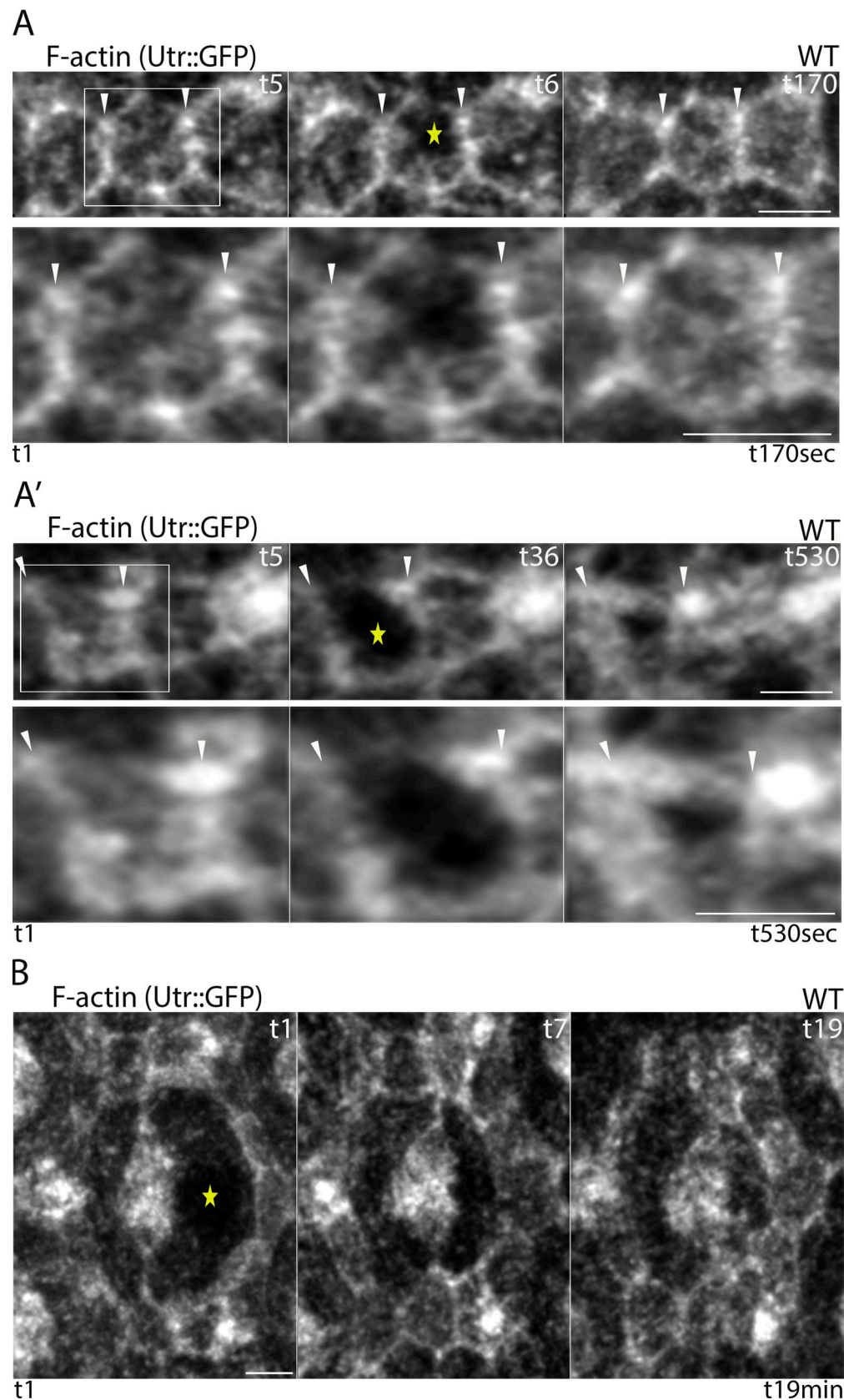
Figure S2. **Medioapical F-actin network can reassemble after ablation. (A and A')** After (A) partial or (A') complete ablation, medioapical F-actin recoils and over time it reassembles. Top: Snapshots of a lattice edge from a time-lapse movie. Bottom: A magnified view of the boxed 2° LC. The yellow star marks the ablated region. White arrowheads mark the LC–LC contact for this and subsequent images. **(B)** Medioapical F-actin in 1° LC also recovers after ablation. Time series montage of F-actin recovery in a 1° LC over a period of 19 min. Scale bar = 3 μm.
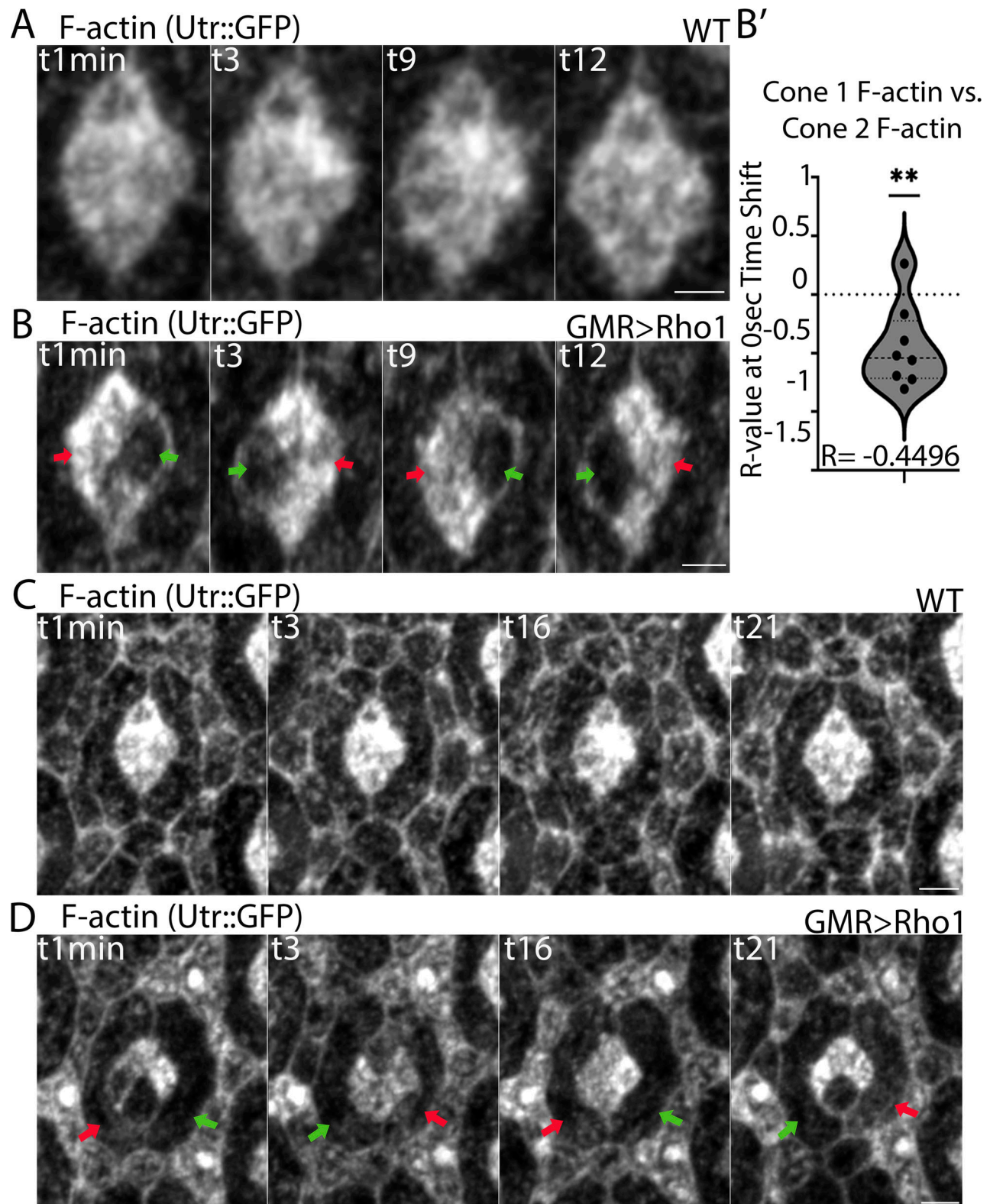
Figure S3. **Anterior and posterior cone cells and 1° cells are mechanically coupled. (A–D)** Rho1 overexpression promotes strong fluctuations in F-actin levels and apical cell area that are inversely coordinated between neighboring cells. **(A and B)** Time series montage showing typical fluctuations in medioapical F-actin and cell area in (A) WT cone cells and (B) cone cells that overexpress Rho1. Green arrows, low F-actin intensity and apical cell area relaxation. Red arrows, high F-actin intensity and apical cell area contraction. **(B')** Fluctuations in F-actin levels are negatively correlated between anterior and posterior cone cells that overexpress Rho1 ($R = -0.4496$, $N = 8$ pairs from 16 cells, one-sample t test: $P = 0.0086$). **(C and D)** Time series montage of medioapical F-actin dynamics and apical cell area fluctuations in (C) WT and (D) Rho1-overexpressing 1° LCs. **(D)** Fluctuations in F-actin and apical cell area also appear negatively correlated between adjacent 1° LCs expressing Rho1. Scale bar = 3 μm.
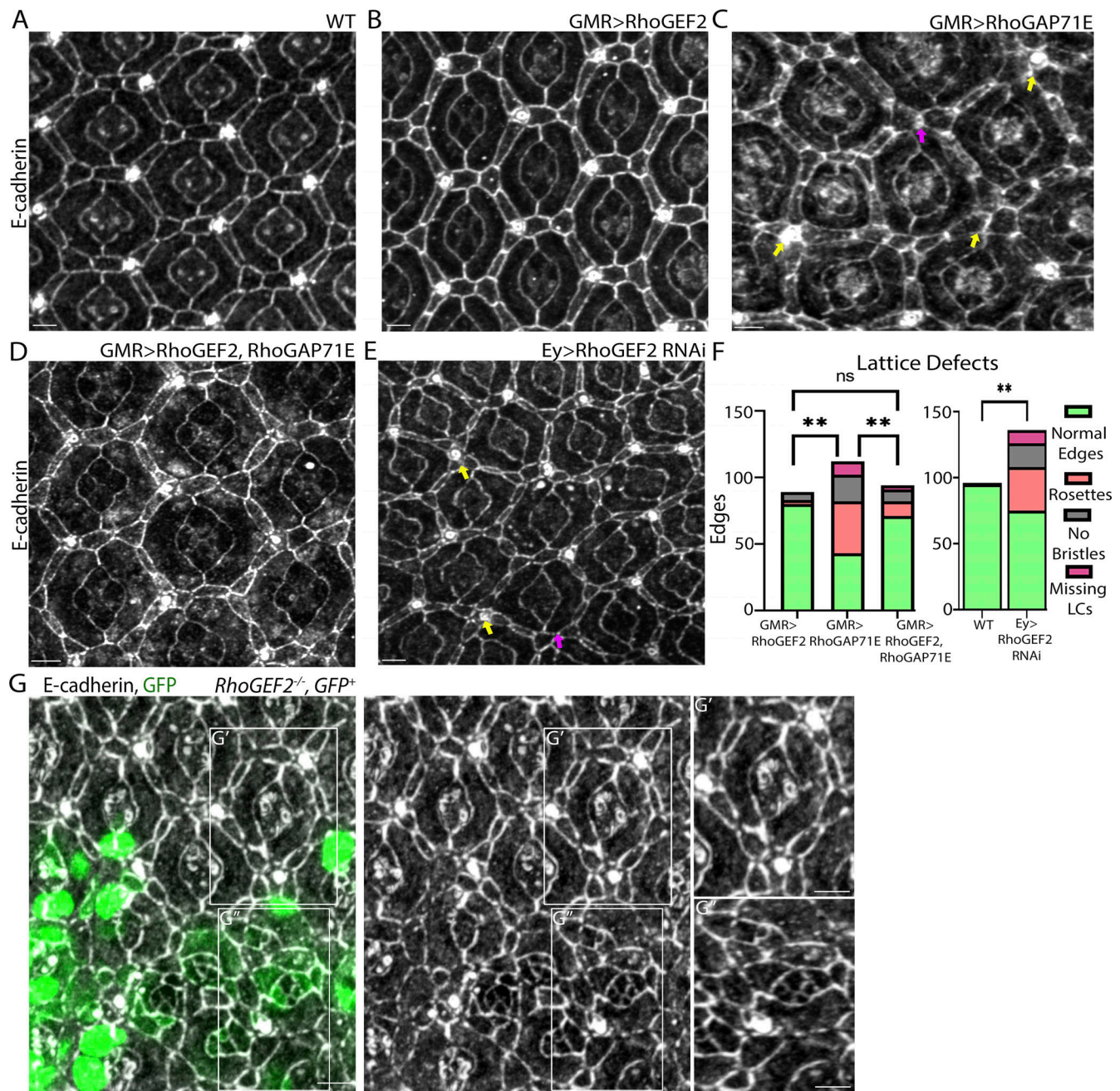
Figure S4. **RhoGEF2 is necessary for formation of ommatidia and remodeling of LCs and can rescue cellular defects caused by RhoGAP71E expression.**
(A) Snapshot of a WT fixed retina stained for E-cad. **(B)** GMR > RhoGEF2-expressing eye. Epithelial cells maintain normal shape and rearrangements. **(C)** GMR > RhoGAP71E induces intercalation defects (yellow arrows), cell loss (purple arrow), and expansion of apical cell area. **(D)** Co-expressing RhoGEF2 and Rho-GAP71E partially rescued the GMR > RhoGAP71E phenotypes. **(E)** RhoGEF2 RNAi expression led to formation of rosettes (yellow arrows) and loss of LCs (purple arrow). **(F)** Quantification of lattice defects. One-way ANOVA with Tukey's multiple comparisons comparing the mean of changes in formation of rosettes. RhoGEF2 versus RhoGAP71E, P = 0.0015. RhoGAP71E versus RhoGEF2/RhoGAP71E, P = 0.0056. RhoGEF2 versus RhoGEF2/RhoGAP71E, P = 0.3789. WT versus Ey-RhoGEF2 RNAi, P = 0.0017. N = 80–140 edges from three eyes. **(G)** Positively marked RhoGEF2 mutant cells in fixed tissue stained for E-cadherin. **(G' and G")** (G) Milder defects are found at the boundary of the clones with WT cells, while (G") severe defects in the formation and structure of ommatidia are found inside the clones. Scale bar = 3 μm.
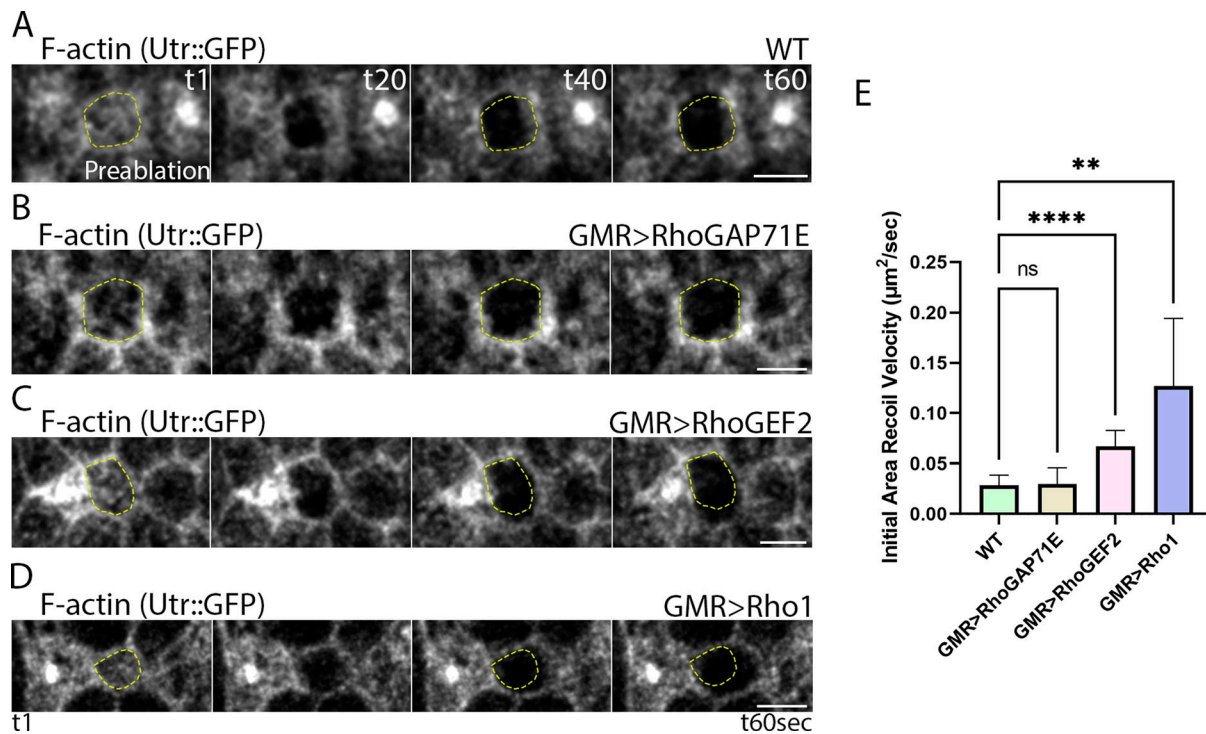
Figure S5. **RhoGEF2 and Rho1 overexpression increase tension in LCs. (A–D)** Time series montage of a lattice edge before and 20, 40, and 60 s after ablating medioapical F-actin (Utr::GFP) in (A) WT, (B) GMR > RhoGAP71E, (C) GMR > RhoGEF2, and (D) GMR > Rho1 expressing retina. Yellow dotted circles highlight the initial cell area before ablation (t1 s panel) and are superimposed over the ablated 2° LCs at t40 and t60 s to highlight the relative cell area change. **(E)** GMR > RhoGEF2 and GMR > Rho1 significantly increased the initial cell area recoil velocity compared with WT cells after ablation. However, we were not able to detect a change in recoil velocities in GMR > RhoGAP71E retina. One-way ANOVA with Dunnett multiple comparisons. WT versus RhoGAP71E, P = 0.9936. WT versus RhoGEF2, P < 0.0001. WT versus Rho1, P = 0.0021. N = 11 for WT in five eyes and Rho1 in four eyes, N = 12 for RhoGAP71E in three eyes and N = 10 for RhoGEF2 in four eyes. Scale bar = 3 μm.
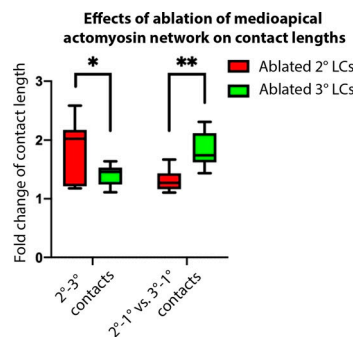

Figure S6. **Preferential impact of 2° and 3° LCs on the length of specific cell–cell contacts.** A comparison of the effects of ablating the medioapical actomyosin network in 2° versus 3° LCs reveals distinct effects on LC–LC (2°-3°) and 2°-1° versus 3°-1° contact expansion. The analysis, conducted using two-way ANOVA with Sídák's multicomparison, demonstrates that ablating the network in 2° LCs has a greater impact on 2°-3° contact expansion than when the network is ablated in 3° LCs (mean R-differences of 0.4388, P = 0.0338, N = 10 from four eyes). Conversely, ablating the network in 3° LCs has a greater effect on 3°-1° versus 2°-1° contact expansion compared with ablating the network in 2° LCs (mean R-differences of 0.5305; P = 0.0095, N = 10 from four eyes).

Video 1. **Medioapical F-actin network dynamics in WT LCs.** Corresponds to Fig. 1. Time-lapse videos of F-actin (Utr::GFP) in WT *Drosophila* LCs that highlight medioapical actomyosin dynamics. Left panel: Yellow arrowheads show the fusion of two F-actin nodes in the 2° LC demarcated by the white box. Right panel: Red arrowhead shows the formation of a medioapical ring-like structure, the subsequent disassembly of the ring, and actin flow to the LC–LC contact (note the green arrowhead movement). Images were acquired every 5 s. Scale bar in this and subsequent movies is 5 μm. The frame rate is 14 frames per second.

Video 2. **Medioapical actomyosin network ablation induces asymmetric cell expansion of the 2° and 3° LCs.** Corresponds to Fig. 2. Time-lapse videos of a 2° (left panel) and a 3° (right panel) LCs with tagged F-actin (Utr::GFP) and MyoII (MyoII::mCh). Targeted ablations of the medioapical actomyosin network in the LCs induced a rapid anisometric apical cell area relaxation (note the area of the 2° and 3° LCs highlighted by the white box before and after ablation). Images were acquired every 1 s. The frame rate is 14 frames per second.

Video 3. **Rho1 expression accelerates medioapical F-actin dynamics and cell area fluctuations in LCs.** Corresponds to Fig. 3. Time-lapse videos of F-actin (Utr::GFP) dynamics in WT fly retina (left panel) and in a retina that overexpresses Rho1 (right panel). Note the robust and accelerated assembly and disassembly of medioapical F-actin in the LCs. This faster turnover of the medioapical actomyosin network is accompanied by a rapid decrease and increase in the apical cell area. Red and green arrowheads highlight the assembly and disassembly of the medioapical actomyosin network, respectively. Images were acquired every 1 min. The frame rate is 14 frames per second.

Video 4. **Medioapical actomyosin network assembly and cell area fluctuations are inversely coordinated between adjacent 2° LCs.** Corresponds to Fig. 3. Time-lapse video of a fly retina that overexpresses Rho1 compared with WT. Rho1 overexpression accelerated the assembly and disassembly of the medioapical F-actin networks and cell area contraction and expansion. Note that this behavior is inversely coordinated between the two neighboring 2° LCs demarcated by the white box. The green arrowhead marks medioapical F-actin assembly; red arrowhead marks disassembly. Images were acquired every 5 s. The frame rate is 14 frames per second.

Video 5. **Constitutive F-actin and MyoII assembly disrupt medioapical actomyosin organization and dynamics.** Corresponds to Fig. 4. Left: Time-lapse video of MyoII (MyoII::mCh) in a MLCK^{CA}-expressing fly eye. Note the rapid assembly and disassembly of a medioapical ring marked with yellow arrowheads. Right: A time-lapse video of F-actin (Utr::GFP) in a Dia^{CA}-expressing eye. Note the increased F-actin levels around the LCs' borders and the low levels and dynamics of medioapical F-actin. Images were acquired every 1 min. The frame rate is 14 frames per second.

Video 6. **RhoGEF2 accelerates medioapical F-actin and MyoII dynamics in LCs.** Corresponds to Fig. 5. Left: A time-lapse video of F-actin (Utr::GFP) in an eye overexpressing RhoGEF2. Note the rapid assembly and disassembly of the medioapical F-actin network marked by the red and yellow arrowheads, respectively. Middle and right: A time-lapse video of MyoII (MyoII::mCh) in clone cells that express a RhoGEF2 RNAi (GFP⁺, white arrowhead) compared with WT counterparts (yellow arrowhead). Right: Note loss of MyoII intensity in the RhoGEF2 RNAi-expressing 2° LC compared with WT. Images were acquired every 5 s. The frame rate is 14 frames per second.

Video 7. **RhoGAP71E inhibits medioapical F-actin and MyoII dynamics in LCs.** Corresponds to Fig. 6. Left: Time-lapse video of F-actin (Utr::GFP) in *Drosophila* eyes that overexpress RhoGAP71E. Note the increased apical cell area of the LCs and reduced medioapical F-actin levels. Middle: Time-lapse video of MyoII (MyoII::mCh) in clones expressing RhoGAP71E RNAi, positively marked with RFP. Right: Note the reduced apical cell area of the RhoGAP71E RNAi-expressing cell (white arrowhead) compared with WT (yellow arrowhead). Images were acquired every 5 s. The frame rate is 14 frames per second.

Video 8. **Rho1 activation is triggered with decreasing tension in expanding LCs, while RhoGAP71E accumulates with increasing tension in contracting cells.** Corresponds to Fig. 7. Time-lapse movie of a sensor for Rho1 activation (AniRBD::GFP) in WT (left) and Rho1-expressing fly eyes (middle). Green arrowheads, expanding cells; red arrowheads, contracting cells. Note the relatively uniform levels of AniRBD in WT and the pulsatile behavior in Rho1 expressing cone cells, with levels increasing in expanding cells and peaking in contracting cells. Right: Time-lapse video of RhoGAP71E::GFP in Rho1-expressing retina. Note the accumulation of RhoGAP71E::GFP in contracting cells and decreased accumulation in expanding cells. Images were acquired every 5 s. The frame rate is 14 frames per second.